

Probing non-minimal coupling through super-horizon instability and secondary gravitational waves

Ayan Chakraborty,^{1,*} Subhasis Maiti,^{1,†} and Debaprasad Maity^{1,‡}

¹*Department of Physics, Indian Institute of Technology, Guwahati, Assam, India*

Abstract

In this paper, we investigate the impact of scalar fluctuations (χ) non-minimally coupled to gravity, $\xi\chi^2R$, as a potential source of secondary gravitational waves (SGWs). Our study reveals that when reheating EoS $w_\phi < 1/3$ and $\xi \lesssim 1/6$ or $w_\phi > 1/3$ and $\xi \gtrsim 1/6$, the super-horizon modes of scalar field experience a *Tachyonic instability* during the reheating phase. Such instability causes a substantial growth in the scalar field amplitude leading to pronounced production of SGWs in the low and intermediate-frequency ranges that are strong enough to be detected by PLANCK and future gravitational wave detectors. Such growth in super-horizon modes of the scalar field and associated GW production may have a significant effect on the strength of the tensor fluctuation at the Cosmic Microwave Background (CMB) scales (parametrized by r) and the number of relativistic degrees of freedom (parametrized by ΔN_{eff}) at the time of CMB decoupling. To prevent such overproduction, the PLANCK constraints on tensor-to-scalar ratio $r \leq 0.036$ and $\Delta N_{\text{eff}} \leq 0.284$ yield a strong lower bound on ξ for $w_\phi < 1/3$, and upper bound on the value of ξ for $w_\phi > 1/3$. Taking into account all the observational constraints we found the value of ξ should be $\gtrsim 0.02$ for $w_\phi = 0$, and $\lesssim 4.0$ for $w_\phi \geq 1/2$ for a wide range of reheating temperature within $10^{-2} \lesssim T_{\text{re}} \lesssim 10^{14}$ GeV, and for a wide range of inflationary energy scales. Further, as one approaches w_ϕ towards $1/3$, the value of ξ remains unconstrained. Finally, we identify the parameter regions in (T_{re}, ξ) plane which can be probed by the upcoming GW experiments namely BBO, DECIGO, LISA, and ET.

Keywords: Scalar Field, Tachyonic Instability, Reheating, Inflation, Secondary Gravitational Waves

arXiv:2408.07767v2 [astro-ph.CO] 5 Oct 2024

*Electronic address: [E-mail:chakrabo@iitg.ac.in](mailto:chakrabo@iitg.ac.in)

†Electronic address: [E-mail: subhashish@iitg.ac.in](mailto:subhashish@iitg.ac.in)

‡Electronic address: [E-mail: debu@iitg.ac.in](mailto:debu@iitg.ac.in)

I. INTRODUCTION

Primordial Gravitational wave (GW) is one of the unique observable predictions of inflationary paradigm [1–14]. Given the advent of a large number of existing [15–27] and upcoming [28–38] GWs detection experiments, inflationary framework proves to be an interesting playground to look for new physics at very high energy scales [39, 40]. Exponential expansion leading to tachyonic growth of the super-horizon modes, and their subsequent evolution are known to be imprinted in the distribution of various cosmological relics such as Cosmic Microwave Background (CMB), Dark Matter (DM), GWs in the form of various correlations of scalar, vector and tensor fluctuations. Over the years enormous efforts have been put into estimating those correlations through the CMB anisotropy ([41] and references therein), dark and baryonic matter distribution [42, 43], and placed tight constraints on the possible physics of inflation. Out of those different relics GW is said to be unique due to its extremely weak (Planck suppressed) but universal coupling. Whereas weak coupling renders it an ideal probe of the very early universe, universal coupling on the other enables it to probe into the nature of all fundamental interactions in both the visible and dark sectors. Utilizing inflation as a mechanism and the subsequent reheating phase, in this paper we intend to probe the non-minimal gravitational coupling $\xi R\chi^2$ with a real scalar field χ through its imprints on the primordial GW spectrum. Such coupling is assumed to be inevitable in the low energy effective theory for the scalar field when coupled with gravity. Non-minimal gravitational coupling has been extensively explored in the context of inflation [44–54], reheating [55–65], DM [66–77], and dark energy [78–81]. In the present paper, however, we focus on exploring the dynamics of super Hubble modes and associated induced GW spectrum. This particular aspect of the present study has been less explored in the literature. Depending on the strength of the non-minimal coupling certain range of super-Hubble modes of the scalar field realize tachyonic growth and may lead to potentially detectable secondary gravitational waves (SGW). Our analysis further reveals that the post-inflationary reheating phase plays an instrumental role. In the perturbative framework, the reheating phase is described by the equation of state w_ϕ of inflaton and reheating temperature T_{re} . The instability that we pointed out for the super Hubble modes turned out to be significantly strong during the reheating phase, particularly for two distinct regions in the (w_ϕ, ξ) parameter space. Whereas for the equation of state $w_\phi < 1/3$, instability arises for $\xi < 1/6$, for $w_\phi > 1/3$, on the other hand, ξ should be greater than the conformal limit $1/6$. Such instability helps enhancing the overall growth of the amplitude of the scalar field modes after they enter into the reheating phase and depends upon the reheating parameters, namely w_ϕ and reheating temperature T_{re} . Further, the cosmological background driven by matter fields with a stiff equation of state is known to amplify GW amplitude when propagating through such background [82]. In this article, we affirm that a combination of the above two non-trivial effects indeed leads to strong GW production for the stiff equation of state. For the $w_\phi < 1/3$, on the other hand, the growth is weaker but GW acquires a non-trivial spectral behavior near the CMB scales that can have an appreciable impact on the tensor-to-scalar ratio. Taking into account CMB constraints on the inflationary tensor power spectrum, and BBN constraints on an effective number of degrees of freedom we demonstrate that SGW induced by non-minimal coupling put a tighter constraint on non-minimal coupling parameters ξ as compared to the values generically assumed in the earlier studies [83–85] and also constraint recently reported considering primary gravitational waves [86]. Maintaining all the existing observational constraints we finally estimate the range of non-minimal coupling against different reheating models that can be probed by the various upcoming GW experiments such as BBO, DECIGO, LISA, and ET.

The order of construction of this paper is as follows. In Section II, we first give a brief overview of the non-perturbative framework of gravitational particle production. We then elaborately discuss the super-horizon instability dynamics (*Tachyonic instability*) of the scalar field in the presence of the non-minimal coupling with gravity $\xi\chi^2R$ and we also compute the associated long-wavelength field solutions during reheating corresponding to three different ranges of non-minimal coupling strength, $0 \leq \xi < 3/16$, $\xi = 3/16$, $\xi > 3/16$ in the entire range of post-inflationary EoS $0 \leq w_\phi \leq 1$. Further, we thoroughly investigate the behavior of the scalar power spectrum and explicitly point out the salient features of this spectrum for varying parameters (w_ϕ, ξ) . We close this section by giving a short discussion on the model-independent definition of the reheating parameters $(N_{\text{re}}, T_{\text{re}})$. In Section III, we discuss the dynamics of the tensor fluctuations with (secondary gravitational waves, SGW) and without (primary gravitational waves, PGW) the anisotropy sourced by the gravitationally produced scalar field. In this section, our prime focus is on the effect of the parametric instability being caused by the non-minimal coupling of the scalar field on the gravitational wave spectrum (PGW+SGW) for both $w_\phi < 1/3$ and $w_\phi > 1/3$. Here we compute the primary as well as the secondary gravitational wave spectrum and show the nature of the full spectrum for varying parameters $(w_\phi, T_{\text{re}}, \xi, r_{0.05})$. Furthermore, we constrain the coupling strength ξ in the light of the present-day tensor-to-scalar ratio at the CMB scale $r_{0.05} \leq 0.036$ and the $\Delta N_{\text{eff}} \leq 0.284$ bound as reported by the recent PLANCK 2018 observation. We also provide a feasible parameter space of the parameter set (T_{re}, ξ) that can be detected by future GW detectors like LISA, DECIGO, BBO, ET, etc. Section IV concludes this paper by shedding light on some possible directions of the present work that are left for future endeavors. In Appendix A, we illustrate the computation of the secondary GW

spectrum for $w_\phi < 1/3$ and $w_\phi > 1/3$, and in Appendix B, we detail the computation of the total energy density of the produced scalar field.

II. SPECTRUM OF GRAVITATIONALLY PRODUCED MASSLESS PARTICLES

We shall begin this section by briefly discussing the basic formalism of non-perturbative particle production. We consider the following general Lagrangian for inflaton (ϕ) and a massive daughter field (χ) non-minimally coupled to gravity and inflaton as follows.

$$\mathcal{L}_{[\phi,\chi]} = -\sqrt{-g} \left(\frac{1}{2} \partial_\mu \phi \partial^\mu \phi + V(\phi) + \frac{1}{2} \partial_\mu \chi \partial^\mu \chi + \frac{1}{2} (m_\chi^2 + g^2 \phi^2 + \xi R) \chi^2 \right). \quad (1)$$

The background FLRW metric is expressed as $ds^2 = a^2(\eta)(-d\eta^2 + d\vec{x}^2)$ with the scale factor a and $\sqrt{-g} = a^4(\eta)$. $V(\phi)$ is the inflaton potential, m_χ^2 is the bare mass of the produced scalar particles. “ ξ ” is the dimensionless non-minimal coupling of χ field with gravity and g is dimensionless coupling strength with the inflaton. Ricci scalar “ R ” generates a time-dependent effective mass for the χ field as, $m_{\text{eff}}^2(\eta) = (m_\chi^2 + g^2 \phi(\eta)^2 + \xi R(\eta))$. Since the background is set by the inflaton which is minimally coupled with gravity, we perform our computation in the Jordon frame for scalar field fluctuation χ .

From the background inflaton part of the Lagrangian (1), we get the inflaton dynamical equation as

$$\phi'' + 2\mathcal{H}\phi' + a^2 \frac{\partial V(\phi)}{\partial \phi} = 0. \quad (2)$$

With the Hubble scale

$$\mathcal{H} = \sqrt{\frac{1}{3M_{\text{pl}}^2} \left(\frac{1}{2} (\phi')^2 + a^2 V(\phi) \right)}, \quad (3)$$

where $\phi' = (d\phi/d\eta)$ and $M_{\text{pl}} = 1/\sqrt{8\pi G} \approx 2.435 \times 10^{18} \text{ GeV}$ is the reduced *Planck* mass. Different dynamical features of inflaton in the Post-inflationary phase influence the Hubble scale which leaves a non-trivial impact on the particle production process.

Expressing the scalar field “ χ ” field in terms of Fourier modes,

$$\chi(\eta, x) = \int \frac{d^3 k}{(2\pi)^3} \chi_k(\eta) e^{ik \cdot x}, \quad (4)$$

and subject to the Lagrangian (1) we reach the following dynamical equation of mode function (χ_k) as,

$$\chi_k'' + 2\mathcal{H}\chi_k' + \left(k^2 + a^2(\eta)(m_\chi^2 + g^2 \phi^2 + \xi R) \right) \chi_k = 0. \quad (5)$$

In the following dynamical Eq. (5), note that there is a damping term, “ $2\mathcal{H}\chi_k'$ ” which is non-zero in expanding background. Defining a new rescaled field $X_k = a(\eta)\chi_k(\eta)$, we obtain the following simplified equation of an oscillator with time-dependent frequency,

$$X_k'' + \left[k^2 + a^2(m_\chi^2 + g^2 \phi^2) + \frac{a^2 R}{6} (6\xi - 1) \right] X_k = 0. \quad (6)$$

The bracketed term in the above Eq. (6) can be identified as a time-dependent frequency “ ω_k ” where,

$$\omega_k^2(\eta) = \left(k^2 + a^2(m_\chi^2 + g^2 \phi^2) + \frac{a^2 R}{6} (6\xi - 1) \right). \quad (7)$$

To solve the Eq. (6) we choose the positive frequency Bunch-Davies vacuum,

$$X_k(\eta_0) = \frac{1}{\sqrt{2\omega_k}} e^{-i\omega_k \eta_0}, \quad X_k'(\eta_0) = -i\sqrt{\frac{\omega_k}{2}} e^{-i\omega_k \eta_0}. \quad (8)$$

Where η_0 is some initial time at which positive-frequency Bunch-Davies vacuum solution is satisfied. The particle occupation number or number density power spectrum for the scalar field is usually expressed as [87],

$$n_k = \frac{1}{2\omega_k} |\omega_k X_k - iX'_k|^2. \quad (9)$$

Integrating Eq.(9) over all the momentum modes, we get the total number and UV convergent energy density as [88, 89]

$$\begin{aligned} n_\chi &= \frac{1}{(2\pi)^3 a^3} \int d^3 k n_k, \\ \rho_\chi &= \frac{1}{(2\pi)^3 a^4} \int d^3 k \omega_k n_k. \end{aligned} \quad (10)$$

The general formalism we constructed in this section is the main foundation of the non-perturbative study of particle production. To this end, we point out that our goal is to analyze the impact of instability due to non-minimal coupling on those modes that remain outside the horizon just after the inflation namely $k < a_{\text{end}} H_{\text{end}}$. Where $(a_{\text{end}}, H_{\text{end}})$ are the scale factor and Hubble scale at the inflation end respectively. On the other hand, from the expression of the effective frequency ω_k one notes that if the $k \gg a_{\text{end}} m_\chi$ condition is satisfied, the bare mass of the χ field can be ignored. Therefore, for the dynamics of the super-horizon modes, the $m_\chi \ll H_{\text{end}}$ condition is equivalent to the massless limit of the scalar field. This is precisely the limit to which we will perform our computation. We further assume that the χ field is non-interacting with the standard model and hence it can be assumed as either dark radiation or dark matter. We have checked that as long as the scalar field mass $m_\chi \lesssim 10^{-5} H_{\text{end}}$, the massless limit is perfectly consistent with our present results. However, the detailed computation for the entire mass range we defer for our future studies.

As just pointed out we consider the massless non-minimally coupled fluctuation which has no other interaction except with gravity. As per these considerations, Lagrangian (1) becomes

$$\mathcal{L}_{[\phi, \chi]} = -\sqrt{-g} \left(\frac{1}{2} \partial_\mu \phi \partial^\mu \phi + V(\phi) + \frac{1}{2} \partial_\mu \chi \partial^\mu \chi + \frac{1}{2} \xi R \chi^2 \right). \quad (11)$$

The scalar field mode equation (6) becomes,

$$X''_{\vec{k}} + \left[k^2 - \frac{a''}{a} (1 - 6\xi) \right] X_{\vec{k}} = 0, \quad (12)$$

where in conformal coordinate, Ricci scalar has been expressed as $R = (6a''/a^3)$. In order to calculate the general solution of the above equation (12), we first need to calculate the *adiabatic vacuum* solution of (12) and any general solution of the equation can then be expressed as a linear combination of that vacuum solution with the knowledge of the *Bogoliev coefficients* α_k and β_k what we shall compute now.

In the present context, we are interested in the spectrum associated with those modes that left the horizon during inflation and again reenter at some point during reheating and later. These long-wavelength modes experience an instability called *Tachyonic instability* after getting out of the horizon during inflation. To take into account the enhancement of field amplitude owing to this instability, we study their dynamics from the early inflationary era to the late reheating phase when all the modes are well inside the horizon. The evolution of scale factor during inflation and reheating with any general EoS can be represented as,

$$a(\eta) = \begin{cases} -\frac{1}{H_{\text{end}} \eta} & -\infty < \eta \leq \eta_{\text{end}} \\ a_{\text{end}} \left(\frac{1+3w_\phi}{2|\eta_{\text{end}}|} \right)^{\frac{2}{1+3w_\phi}} \left(\eta - \eta_{\text{end}} + \frac{2|\eta_{\text{end}}|}{1+3w_\phi} \right)^{\frac{2}{1+3w_\phi}} & \eta \geq \eta_{\text{end}} \end{cases}. \quad (13)$$

Considering pure de-Sitter inflation, we assume the Hubble scale at the end of inflation as H_{end} . It is straightforward to check that during the transition from inflation to reheating, the scale factor and its first derivative change continuously at the junction point, that is at the end of inflation, $\eta = \eta_{\text{end}} = -(1/a_{\text{end}} H_{\text{end}})$. Here a_{end} is the scale factor at $\eta = \eta_{\text{end}}$ and w_ϕ is the background inflaton EoS during reheating.

Associated Hubble scale behaves as

$$\mathcal{H}(\eta \geq \eta_{\text{end}}) = \frac{a'(\eta)}{a(\eta)} = \frac{2(a_{\text{end}} H_{\text{end}})}{(1+3w_\phi)} \left((\eta a_{\text{end}} H_{\text{end}}) + \frac{3(1+w_\phi)}{(1+3w_\phi)} \right)^{-1} \quad (14)$$

It is well-known that the violation of the adiabaticity condition owing to the changing background geometry in the abrupt transition from de-Sitter vacuum to post-inflationary vacuum state causes particle production associated with long-wavelength modes. In particular, one defines a dimensionless factor $|\omega'_k/\omega_k^2|$ to study the departure from the adiabatic limit and in the process of transition, this adiabaticity condition gets violated ($|\omega'_k/\omega_k^2| \gg 1$) at some intermediate point giving a burst of particles in long-wavelength regime.

Now let us suppose $X_k^{(\text{inf})}(\eta)$ is the adiabatic vacuum solution of (12) during the de-Sitter phase in the time interval $-\infty < \eta \leq \eta_{\text{end}}$ and $X_k^{(\text{reh})}(\eta)$ is the adiabatic vacuum solution during reheating phase for $\eta \geq \eta_{\text{end}}$. Any general field solution during reheating can thus be expressed as

$$X_k(\eta) = \alpha_k X_k^{(\text{reh})} + \beta_k X_k^{*(\text{reh})}, \quad (15)$$

where, (α_k, β_k) can be identified as Bogoliubov coefficients. Making these solutions and their first derivatives continuous at the junction $\eta = \eta_{\text{end}}$, we compute the Bogoliubov coefficients as follows: [90]

$$\begin{aligned} \alpha_k &= i \left(X_k^{(\text{inf})'}(\eta_{\text{end}}) X_k^{(\text{reh})*}(\eta_{\text{end}}) - X_k^{(\text{inf})}(\eta_{\text{end}}) X_k^{(\text{reh})*' }(\eta_{\text{end}}) \right), \\ \beta_k &= -i \left(X_k^{(\text{inf})'}(\eta_{\text{end}}) X_k^{(\text{reh})}(\eta_{\text{end}}) - X_k^{(\text{reh})'}(\eta_{\text{end}}) X_k^{(\text{inf})}(\eta_{\text{end}}) \right), \end{aligned} \quad (16)$$

where $(')$ denotes the derivative with respect to conformal time.

Now, our goal would be to obtain the adiabatic vacuum solutions in both the phases. Using the scale factor (13) in the equation (12), we obtain the form of the dynamical equation during de-Sitter inflation ($\eta \leq \eta_{\text{end}}$) as,

$$X_k'' + \underbrace{\left[k^2 - \frac{2(1-6\xi)}{\eta^2} \right]}_{\omega_k^2} X_k = 0. \quad (17)$$

From the above equation it can be noted that long wavelength modes after their horizon crossing becomes tachyonic ($\omega_k^2 < 0$) for $0 \leq \xi < 1/6$. As ξ exceeds the conformal limit $\xi = 1/6$, this instability ceases to exist.

The general solution of this equation is

$$X_k = C_1 \sqrt{|\eta|} J_{\nu_1}(k|\eta|) + C_2 \sqrt{|\eta|} Y_{\nu_1}(k|\eta|). \quad (18)$$

With the order of the Bessel functions $\nu_1 = \sqrt{9-48\xi}/2$ and C_1, C_2 are integration constants. To evaluate α_k and β_k , we need to define first the vacuum solution $X_k^{(\text{inf})}$ during inflation. To compute the de-Sitter vacuum solution, we use the Bunch-Davies vacuum condition at the beginning of inflation. In this limit $k|\eta| \gg 1$, the mode solution (18) becomes,

$$X_k(\eta) \sim \frac{1}{\sqrt{2\pi k}} \left[(C_1 - iC_2) e^{-i(k\eta + \pi/4 + \pi\nu_1/2)} + (C_1 + iC_2) e^{i(k\eta + \pi/4 + \pi\nu_1/2)} \right]. \quad (19)$$

In the asymptotic in-vacuum limit, the positive-frequency outgoing mode function behaves as

$$X_k(\eta) \xrightarrow{\eta \rightarrow -\infty} \frac{e^{-ik\eta}}{\sqrt{2k}}. \quad (20)$$

Comparing (19) with (20) we have

$$C_1 = \frac{\sqrt{\pi}}{2} e^{i(\pi/4 + \pi\nu_1/2)}, \quad C_2 = \frac{i\sqrt{\pi}}{2} e^{i(\pi/4 + \pi\nu_1/2)}. \quad (21)$$

Therefore, the adiabatic vacuum solution during de-Sitter inflation is

$$X_k^{(\text{inf})} = \frac{\sqrt{-\pi\eta}}{2} e^{i(\pi/4 + \pi\nu_1/2)} H_{\nu_1}^{(1)}(-k\eta). \quad (22)$$

Similarly the dynamical equation for general post-inflationary ($\eta > \eta_{\text{end}}$) EoS “ w_ϕ ” is

$$X_k'' + \underbrace{\left[k^2 - \frac{2(1-3w_\phi)(1-6\xi)}{(1+3w_\phi)^2 \left(\eta + \frac{3(1+w_\phi)}{a_{\text{end}} H_{\text{end}} (1+3w_\phi)} \right)^2} \right]}_{\omega_k^2} X_k = 0, \quad (23)$$

From the above equation, it can be again noted that the modes which were stable during inflation for $\xi > 1/6$ become tachyonic ($\omega_k^2 < 0$) during reheating for $w_\phi > 1/3$ [68]. We will see that this will play a significant role in our subsequent studies. The general solution of this equation is

$$X_k(\eta) = C_3 4^{\nu_2} \Gamma(\nu_2 + 1) \sqrt{2ik\bar{\eta}} I_{\nu_2}(ik\bar{\eta}) + C_4 \sqrt{\frac{2ik\bar{\eta}}{\pi}} K_{\nu_2}(ik\bar{\eta}). \quad (24)$$

Where we use the symbol $\bar{\eta} = (\eta + 3\mu/a_{\text{end}}H_{\text{end}})$. I_{ν_2} and K_{ν_2} are modified Bessel functions of order ν_2 with

$$\mu = \frac{(1 + w_\phi)}{(1 + 3w_\phi)}, \quad \nu_2 = \frac{\sqrt{3(1 + w_\phi)(3(1 - w_\phi)^2 + 16\xi(3w_\phi - 1))}}{2\sqrt{1 + 3w_\phi}\sqrt{1 + 4w_\phi + 3w_\phi^2}}. \quad (25)$$

and C_3, C_4 are the integration constants.

We now seek the solution of (23) compatible with the requirements of an adiabatic vacuum. If spacetime changes very slowly or equivalently particle momentum is so large that it hardly feels the background dynamics, the mode function can be safely assumed to behave as a positive frequency mode in Minkowski space in its asymptotic limit. For this we assume the ($k\eta \gg 1$) limit, and the mode solution (24) transforms into,

$$X_k(\eta) \sim \left[C_3 \frac{2^{2\nu_2} \Gamma(\nu_2 + 1)}{\sqrt{\pi}} e^{ik\bar{\eta}} + C_4 e^{-ik\bar{\eta}} \right]. \quad (26)$$

In the adiabatic out-vacuum limit that is for $\eta \gg 1$ or equivalently $a(\eta) \rightarrow \infty$ mode function behaves as a positive frequency state

$$X_k(\eta) \xrightarrow{\eta \rightarrow \infty} \frac{e^{-ik\eta}}{\sqrt{2k}}, \quad (27)$$

Comparing (26) with (27) we have

$$C_3 = 0, \quad C_4 = \frac{1}{\sqrt{2k}} \exp\left[\frac{3ik\mu}{a_{\text{end}}H_{\text{end}}}\right]. \quad (28)$$

Therefore, the adiabatic vacuum solution of massless particles for general reheating EoS “ w_ϕ ” becomes

$$X_k^{(\text{reh})}(\eta) = \sqrt{\frac{\bar{\eta}}{\pi}} \exp\left[\frac{3ik\mu}{a_{\text{end}}H_{\text{end}}} + \frac{i\pi}{4}\right] K_{\nu_2}(ik\bar{\eta}). \quad (29)$$

It is important to note that depending upon the value of the non-minimal coupling constant ξ , the order of the inflationary vacuum solution ν_1 becomes positive for $0 \leq \xi < 3/16$, zero for $\xi = 3/16$, and imaginary for $\xi > 3/16$. In addition to this, the index of post-inflationary vacuum solution ν_2 also becomes imaginary in the range $\xi > 3/16$ for EoS $0 \leq w_\phi < 1/3$ and it becomes real positive for $1/3 \leq w_\phi \leq 1$. This varying nature of the indices ν_1, ν_2 depending upon different ranges of non-minimal coupling strength and post-inflationary EoS greatly influences the nature of the post-inflationary field solution. Now we shall compute the field solution during reheating for general EoS in three specified ranges of the non-minimal coupling strength ξ .

A. Field solution at large scale for $0 \leq w_\phi < 1/3$

1. For $0 \leq \xi < 3/16$:

As mentioned earlier, the general field solution in a particular phase can be expressed as a linear combination of the respective vacuum solution with the help of Bogoliubov coefficients α_k and β_k (See Eq.(15)). So, our main task is to compute α_k and β_k using the relations in (16). In this specified range of ξ we get both ν_1 and ν_2 to be positive definite. Substituting these vacuum solutions (22) and (29) into (16), in long-wavelength limit $k/k_{\text{end}} \ll 1$, we compute the Bogoliubov coefficients as

$$\alpha_k \approx \frac{\Gamma(\nu_1)\Gamma(\nu_2)2^{\nu_1}}{8\pi} \left(\frac{2}{3\mu - 1}\right)^{\nu_2} \left(\frac{3\mu(1 - 2\nu_1) + 2(\nu_1 - \nu_2)}{\sqrt{(3\mu - 1)}}\right) \left(\frac{1}{\bar{k}}\right)^{\nu_1 + \nu_2} e^{i\left(\frac{\pi\nu_1}{2} + \frac{\pi\nu_2}{2} + \frac{\pi}{2} - 3\mu\bar{k}\right)}$$

$$\beta_k \approx \alpha_k e^{i(-\pi\nu_2 - \frac{\pi}{2} + 6\mu\bar{k})} \quad (30a)$$

For simplified expression we define a new symbol $\bar{k} = k/k_{\text{end}}$. We define the energy density of the produced particles at a time during reheating when the associated longest wavelength is well inside the horizon. In this sense, we always have $k\eta \gg 1$ for any mode which will contribute to the energy density. Using the long-wavelength approximated form of the coefficients α_k and β_k (See Eq.(30)) in (15) we obtain the general long-wavelength solution of scalar field for general EoS in the specified ξ range for $k\eta \gg 1$ as

$$X_k^{\text{long}}(\eta) \approx \frac{\Gamma(\nu_1)\Gamma(\nu_2)2^{\nu_1}}{4\pi\sqrt{k_{\text{end}}}} \left(\frac{2}{3\mu-1}\right)^{\nu_2} \left(\frac{3\mu(1-2\nu_1)+2(\nu_1-\nu_2)}{\sqrt{2(3\mu-1)}}\right) \frac{\cos(k\eta)}{\bar{k}^{(\nu_1+\nu_2+1/2)}} \quad (31)$$

where $k_{\text{end}} = a_{\text{end}}H_{\text{end}}$ is the scale that leaves the horizon at the end of inflation.

2. For $\xi = 3/16$:

For this particular value of the coupling strength ξ , ν_1 vanishes. Following the same procedure, in the long-wavelength limit, α_k and β_k can now be evaluated as

$$\alpha_k \approx -\frac{\Gamma(\nu_2)}{2} \left(\frac{2}{3\mu-1}\right)^{\nu_2} \left(\frac{3\mu-2\nu_2}{4\sqrt{3\mu-1}} + \frac{i\sqrt{3\mu-1}}{\pi}\right) \frac{\exp(i(\pi\nu_2/2 - \pi/2 - 3\mu\bar{k}))}{\bar{k}^{\nu_2}} \quad (32a)$$

$$\beta_k \approx \frac{\Gamma(\nu_2)}{2} \left(\frac{2}{3\mu-1}\right)^{\nu_2} \left(\frac{3\mu-2\nu_2}{4\sqrt{3\mu-1}} + \frac{i\sqrt{3\mu-1}}{\pi}\right) \frac{\exp(i(-\pi\nu_2/2 + 3\mu\bar{k}))}{\bar{k}^{\nu_2}} \quad (32b)$$

Associated general field solution for $\xi = 3/16$ in $k\eta \gg 1$ limit becomes

$$X_k^{\text{long}}(\eta) \approx \frac{\Gamma(\nu_2)}{\sqrt{2k_{\text{end}}}} \left(\frac{2}{3\mu-1}\right)^{\nu_2} \left(\frac{3\mu-2\nu_2}{4\sqrt{3\mu-1}} + \frac{i\sqrt{3\mu-1}}{\pi}\right) \frac{i\sin(k\eta)}{\bar{k}^{\nu_2+1/2}} \quad (33)$$

3. For $\xi > 3/16$:

In this range of ξ values, ν_1 and ν_2 become imaginary. Long-wavelength approximated Bogolieubov coefficients are

$$\alpha_k \approx \left(K_{\nu_2} \left(i\bar{k}(3\mu-1) \right) H_{\nu_1}^{(1)}(\bar{k}) \left(\frac{3\mu}{\sqrt{3\mu-1}} \right) + \bar{k}\sqrt{3\mu-1} \left(H_{\nu_1-1}^{(1)}(\bar{k}) - H_{\nu_1+1}^{(1)}(\bar{k}) \right) \right) \times \exp(i(\pi/2) - 3\mu\bar{k}) \frac{\exp(-\pi\tilde{\nu}_1/2)}{4} \quad (34a)$$

$$\beta_k \approx \left(K_{\nu_2} \left(i\bar{k}(3\mu-1) \right) H_{\nu_1}^{(1)}(\bar{k}) \left(\frac{3\mu}{\sqrt{3\mu-1}} \right) + \bar{k}\sqrt{3\mu-1} \left(H_{\nu_1-1}^{(1)}(\bar{k}) - H_{\nu_1+1}^{(1)}(\bar{k}) \right) \right) \times \exp(3\mu\bar{k}) \frac{\exp(-\pi\tilde{\nu}_1/2)}{4} \quad (34b)$$

General field solution for $\xi > 3/16$ becomes

$$X_k^{\text{long}}(\eta) \approx \frac{\exp(-\pi\tilde{\nu}_1/2)}{4\sqrt{2k_{\text{end}}}} \left(K_{\nu_2} \left(i\bar{k}(3\mu-1) \right) H_{\nu_1}^{(1)}(\bar{k}) \left(\frac{3\mu}{\sqrt{3\mu-1}} \right) + \bar{k}\sqrt{3\mu-1} \left(H_{\nu_1-1}^{(1)}(\bar{k}) - H_{\nu_1+1}^{(1)}(\bar{k}) \right) \right) \frac{\cos(k\eta)}{\bar{k}^{1/2}} \quad (35)$$

where $\tilde{\nu}_1 = (\sqrt{48\xi - 9})/2$.

B. Field solution at large scale for $1/3 \leq w_\phi \leq 1$

1. For $0 \leq \xi < 3/16$:

Likewise in the previous case, the indices ν_1, ν_2 are also real positive in this EoS range. In the limit $k/k_{\text{end}} \ll 1$, using equations (22),(29), and (16), we obtain Bogoliebov coefficients as

$$\alpha_k \approx -\frac{\Gamma(\nu_1)\Gamma(\nu_2)2^{\nu_1}}{8\pi} \left(\frac{2}{3\mu-1}\right)^{\nu_2} \left(\frac{3\mu(1-2\nu_1)+2(\nu_1-\nu_2)}{\sqrt{(3\mu-1)}}\right) \frac{\exp(i(\pi\nu_1/2 + \pi\nu_2/2 - \pi/2 - 3\mu\bar{k}))}{\bar{k}^{(\nu_1+\nu_2)}} \quad (36a)$$

$$\beta_k \approx \frac{\Gamma(\nu_1)\Gamma(\nu_2)2^{\nu_1}}{8\pi} \left(\frac{2}{3\mu-1}\right)^{\nu_2} \left(\frac{3\mu(1-2\nu_1)+2(\nu_1-\nu_2)}{\sqrt{(3\mu-1)}}\right) \frac{\exp(i(\pi\nu_1/2 - \pi\nu_2/2 + 3\mu\bar{k}))}{\bar{k}^{(\nu_1+\nu_2)}} \quad (36b)$$

Subject to the following coefficients, the general field solution in $k\eta \gg 1$ limit becomes

$$X_k^{\text{long}}(\eta) \approx \frac{\Gamma(\nu_1)\Gamma(\nu_2)2^{\nu_1}}{4\pi\sqrt{k_{\text{end}}}} \left(\frac{2}{3\mu-1}\right)^{\nu_2} \left(\frac{3\mu(1-2\nu_1)+2(\nu_1-\nu_2)}{\sqrt{2(3\mu-1)}}\right) \frac{i\sin(k\eta)}{\bar{k}^{(\nu_1+\nu_2+1/2)}} \quad (37)$$

2. For $\xi = 3/16$:

For this particular value of ξ , the expression of Bogoliebov coefficients as well as general field solution will remain same for this EoS range $1/3 \leq w_\phi \leq 1$ also. Here also we obtain α_k and β_k as

$$\alpha_k \approx -\frac{\Gamma(\nu_2)}{2} \left(\frac{2}{3\mu-1}\right)^{\nu_2} \left(\frac{3\mu-2\nu_2}{4\sqrt{(3\mu-1)}} + \frac{i\sqrt{3\mu-1}}{\pi}\right) \frac{\exp(i(\pi\nu_2/2 - \pi/2 - 3\mu\bar{k}))}{\bar{k}^{\nu_2}} \quad (38a)$$

$$\beta_k \approx \frac{\Gamma(\nu_2)}{2} \left(\frac{2}{3\mu-1}\right)^{\nu_2} \left(\frac{3\mu-2\nu_2}{4\sqrt{(3\mu-1)}} + \frac{i\sqrt{3\mu-1}}{\pi}\right) \frac{\exp(i(-\pi\nu_2/2 + 3\mu\bar{k}))}{\bar{k}^{\nu_2}} \quad (38b)$$

Associated general field solution for $\xi = 3/16$ in $k\eta \gg 1$ limit will be

$$X_k^{\text{long}}(\eta) \approx \frac{\Gamma(\nu_2)}{\sqrt{2k_{\text{end}}}} \left(\frac{2}{3\mu-1}\right)^{\nu_2} \left(\frac{3\mu-2\nu_2}{4\sqrt{(3\mu-1)}} + \frac{i\sqrt{3\mu-1}}{\pi}\right) \frac{i\sin(k\eta)}{\bar{k}^{\nu_2+1/2}} \quad (39)$$

3. For $\xi > 3/16$:

A significant difference in terms of spectral behavior will appear between two given EoS ranges in this particular case $\xi > 3/16$. In this case, we get one index ν_1 to be imaginary as expected but another index ν_2 to be real positive which differs from the previous case for $0 \leq w_\phi < 1/3$. This causes a noticeable change in the spectral behavior as we see soon. Long-wavelength approximated coefficients are evaluated to be

$$\alpha_k \approx \frac{\Gamma(\nu_2)\exp(-\pi\tilde{\nu}_1/2)}{8} \left(\frac{3\mu-2\nu_2}{\sqrt{(3\mu-1)}} H_{\nu_1}^{(1)}(\bar{k}) + \bar{k}\sqrt{3\mu-1} (H_{\nu_1-1}^{(1)}(\bar{k}) - H_{\nu_1+1}^{(1)}(\bar{k}))\right) \times \frac{\exp(i(\pi\nu_2/2 + \pi/2 - 3\mu\bar{k}))}{\bar{k}^{\nu_2}} \left(\frac{2}{3\mu-1}\right)^{\nu_2} \quad (40a)$$

$$\beta_k \approx \frac{\Gamma(\nu_2)\exp(-\pi\tilde{\nu}_1/2)}{8} \left(\frac{3\mu-2\nu_2}{\sqrt{(3\mu-1)}} H_{\nu_1}^{(1)}(\bar{k}) + \bar{k}\sqrt{3\mu-1} (H_{\nu_1-1}^{(1)}(\bar{k}) - H_{\nu_1+1}^{(1)}(\bar{k}))\right) \times \frac{\exp(i(3\mu\bar{k} - \pi\nu_2/2))}{\bar{k}^{\nu_2}} \left(\frac{2}{3\mu-1}\right)^{\nu_2} \quad (40b)$$

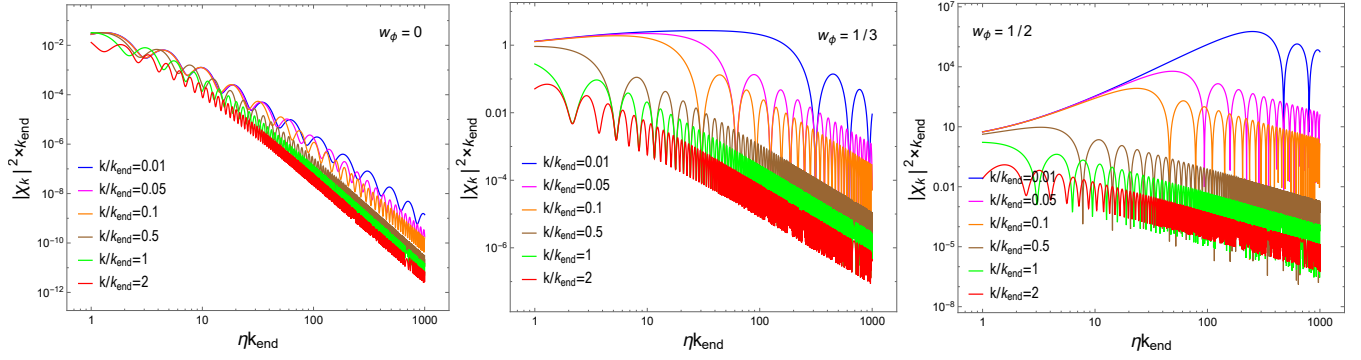


FIG. 1: Figure represents the time-evolution of dimensionless field amplitude square ($|\chi_k|^2 \times k_{\text{end}}$) associated with some large scale ($k < k_{\text{end}}$) and small scale ($k > k_{\text{end}}$) modes for three different EoS. In all three plots, we choose the non-minimal coupling strength to be $\xi = 3$. It is clearly seen that for $\xi > 1/6$, the post-inflationary instability effect associated with long-wavelength modes is effective for $w_\phi > 1/3$ as discussed earlier.

Therefore, the associated general field solution takes the following form.

$$X_k^{\text{long}}(\eta) \approx \frac{\Gamma(\nu_2) \exp(-\pi \tilde{\nu}_1/2)}{4\sqrt{2k_{\text{end}}}} \left(\frac{3\mu - 2\nu_2}{\sqrt{(3\mu - 1)}} H_{\nu_1}^{(1)}(\bar{k}) + \bar{k} \sqrt{3\mu - 1} (H_{\nu_1 - 1}^{(1)}(\bar{k}) - H_{\nu_1 + 1}^{(1)}(\bar{k})) \right) \times \frac{\cos(k\eta)}{\bar{k}^{\nu_2 + 1/2}} \left(\frac{2}{3\mu - 1} \right)^{\nu_2} \quad (41)$$

From our analysis so far it is revealed that the long-wavelength scalar field modes gets amplified through tachyonic instability during and after inflation depending upon the value of (ξ, w_ϕ) . To this end let us reiterate again that for $0 \leq \xi < 1/6$ long wavelength modes after their horizon crossing during inflation, get amplified due to tachyonic instability effect (see Eq.(17)). As ξ exceeds the conformal limit $\xi = 1/6$, the inflationary instability diminishes, whereas new tachyonic instability develops during reheating, particularly for stiff equation of state $w_\phi > 1/3$ (see Eq.(23)). Enhancement of the scalar field modes due to those instabilities can indeed be observed in Fig.1. In the figure we have plotted the time evolution of different field modes assuming $\xi = 3$ for three different equations of state $w_\phi = (0, 1/3, 1/2)$. It can indeed be seen that for $\xi > 1/6, w_\phi > 1/3$, the amplitude of the original field modes χ_k increases appreciably.

The excitation of these large-scale modes due to the instability effect during and after inflation for different parameter regions of ξ and w_ϕ motivates us to investigate the induced GWs. In the subsequent study of the generation of secondary GWs sourced by the anisotropy, we pay attention to the long-wavelength modes of the source, that lie in the range $k_* < k < k_{\text{end}}$ where $(k_*/a_0) = 0.05 \text{Mpc}^{-1}$ is the present-day CMB pivot scale.

C. Behavior of scalar field energy density spectrum “ $\rho_{\chi_k}(\eta)$ ”

While defining the anisotropic stress tensor later, we require the nature of the power spectrum of the source field(χ). However, we shall soon see in the subsequent section that the gravitational wave energy density spectrum follows the spectral behavior of the field energy density spectrum(ρ_{χ_k}) in the long-wavelength regime $k \ll k_{\text{re}}$. According to the standard definition given in [13], we define the field power spectrum of the produced fluctuations corresponding to the original field mode χ_k as $\mathcal{P}_\chi(k, \eta) = \frac{k^3}{2\pi^2 a^2} |X_k|^2$. Excluding the non-minimal coupling term, the standard expression of energy density in terms of rescaled field mode(X_k) and its derivative(X'_k) is $\rho_\chi = \frac{1}{4\pi^2 a^4} \int d(\ln k) k^3 (|X'_k|^2 + k^2 |X_k|^2)$ [71, 72]. Hence associated energy density spectrum can be expressed as $\rho_{\chi_k}(\eta) = \frac{k^3}{4\pi^2 a^4} (|X'_k|^2 + k^2 |X_k|^2) = (k^2/a^2) \mathcal{P}_\chi(k, \eta)$. Now we shall discuss the spectral features of ρ_{χ_k} in the entire post-inflationary EoS range $0 \leq w_\phi \leq 1$ for three different ξ ranges.

1. For $0 \leq w_\phi < 1/3$:

$$\rho_{\chi_k}(\eta > \eta_{\text{end}}) = \frac{k^2}{a^2} \mathcal{P}_\chi(k, \eta > \eta_{\text{end}}) \propto \begin{cases} (\cos^2(k\eta)/a(\eta)^4)(k/k_{\text{end}})^{2(2-\nu_1-\nu_2)} & \text{for } 0 \leq \xi < 3/16 \\ (\sin^2(k\eta)/a(\eta)^4)(k/k_{\text{end}})^{2(2-\nu_2)} & \text{for } \xi = 3/16 \\ (1/a(\eta)^4)(k/k_{\text{end}})^4 & \text{for } \xi > 3/16 \end{cases} \quad (42)$$

2. For $1/3 \leq w_\phi \leq 1$:

$$\rho_{\chi_k}(\eta > \eta_{\text{end}}) \propto \begin{cases} (\sin^2(k\eta)/a(\eta)^4)(k/k_{\text{end}})^{2(2-\nu_1-\nu_2)} & \text{for } 0 \leq \xi < 3/16 \\ (\sin^2(k\eta)/a(\eta)^4)(k/k_{\text{end}})^{2(2-\nu_2)} & \text{for } \xi = 3/16 \\ (\cos^2(k\eta)/a(\eta)^4)(k/k_{\text{end}})^{2(2-\nu_2)} & \text{for } \xi > 3/16 \end{cases} \quad (43)$$

Depending upon EoS in three ranges $0 \leq w_\phi < 1/3$, $w_\phi = 1/3$, and $1/3 \leq w_\phi \leq 1$, the scalar field energy density spectrum $\rho_{\chi_k}(\eta)$ has interesting spectral behavior with the variation of coupling strength ξ . We first illustrate those important features of the $\rho_{\chi_k}(\eta)$ spectrum at a fixed time (and this is true for any time) for varying EoS w_ϕ in different ranges of ξ values. We shall next discuss the behavior of the spectrum at varying instants of time for a fixed coupling strength.

3. Spectral behavior of “ $\rho_{\chi_k}(\eta)$ ” at a fixed time :

We first study the nature of the energy density spectrum for varying coupling strength at a fixed time during reheating.

- For $0 \leq w_\phi < 1/3$: Examining the spectrum as given in (42) for $0 \leq w_\phi < 1/3$, we find that for $0 \leq \xi < 1/6$, the spectrum is always red-tilted or IR divergent $\rho_{\chi_k}(\eta) \propto k^{2(2-\nu_1-\nu_2)}$ with $(2 - \nu_1 - \nu_2) < 0$. However, the amount of red tilt depends upon the choice of EoS w_ϕ through the following relations,

$$\nu_1 = \frac{\sqrt{9 - 48\xi}}{2} \quad ; \quad \nu_2 = \frac{\sqrt{3(1 + w_\phi)(3(1 - w_\phi)^2 + 16\xi(3w_\phi - 1))}}{2\sqrt{1 + 3w_\phi}\sqrt{1 + 4w_\phi + 3w_\phi^2}}. \quad (44)$$

With the above mentioned parameter ranges ν_2 should lie within $\sqrt{9 - 48\xi}/2 > \nu_2 > 1/2$. For example, as w_ϕ approaches zero the spectrum becomes maximally red-tilted $\rho_{\chi_k}(\eta) \propto k^{2(2-2\nu_1)}$ for given $\xi < 1/6$ up to the sinusoidal function of k . Such red tilt can indeed be observed in the blue curve in the left panel of Fig.2. Furthermore, there exists a critical coupling strength ξ_{cri} lying in this range $0 < \xi_{\text{cri}} < 1/6$, at which energy spectrum becomes scale-invariant giving $(4 - 2(\nu_1 + \nu_2)) = 0$ (see the magenta line in the left panel of Fig.2). Therefore, for $0 < \xi_{\text{cri}} < 1/6$, energy spectrum remains IR divergent in the range $0 \leq \xi < \xi_{\text{cri}}$ and it turns blue-tilted $(4 - 2(\nu_1 + \nu_2)) > 0$ for $\xi > \xi_{\text{cri}}$. Due to this red-tilted behavior of the energy density spectrum, the gravitational wave amplitude would be very large at the CMB scale. The PLANCK constraint on tensor to scalar ratio $r_{0.05} < 0.036$ will, therefore be shown to set a lower limit on the value of ξ . Once ξ exceeds conformal limit $\xi > 1/6$, the spectrum remains blue-tilted till one reaches the $\xi = 3/16$. As ξ exceeds $3/16$, both the indices ν_1, ν_2 being imaginary results in the energy density spectrum to be insensitive to the non-minimal coupling strength with $\rho_{\chi_k}(\eta) \propto k^4$. In the left panel of Fig.2 we can indeed see the blue titled spectrum for $\xi = (3/16, 1, 4)$ in brown, green and red respectively. In summary, in the entire range of $\xi > \xi_{\text{cri}}$, the spectrum being blue-tilted draws the maximum contribution to the amplitude of the scalar power spectrum amplitude for those modes which left the horizon at the inflation end, that is k_{end} .

- For $w_\phi = 1/3$: For this particular value of the equation of state, $\nu_2 = 1/2$, irrespective of the choice of ξ , and in the range $0 \leq \xi < 1/6$, ν_1 lies within $[3/2, 1/2)$. Consequently, we obtain a scale-invariant energy density spectrum (see the blue line in the middle panel of Fig.2) for $\xi = 0$, and a blue-tilted spectrum in the range $0 < \xi < 1/6$. As ξ exceeds the conformal limit, the index ν_1 gradually decreases with the increase of ξ up to

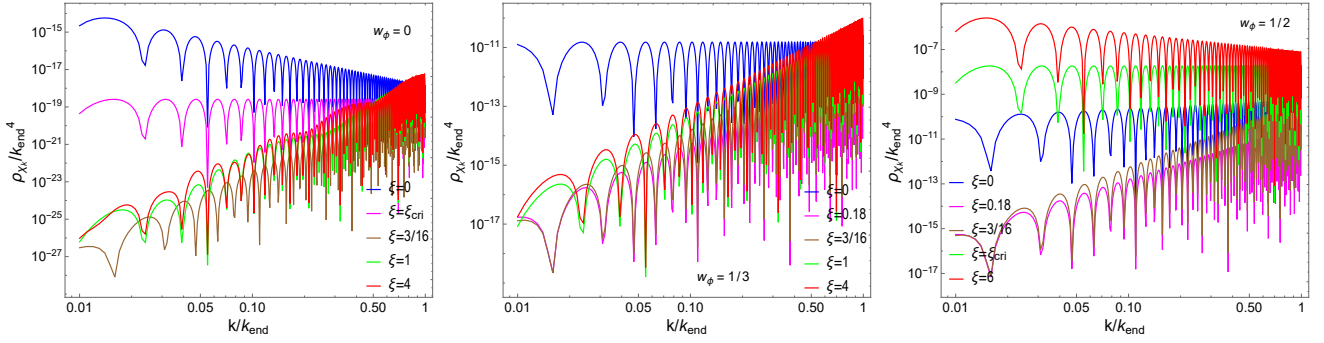


FIG. 2: Figure represents the variation of dimensionless scalar field energy density spectrum $\rho_{\chi_k}(\eta)/k_{\text{end}}^4$ with non-minimal coupling strength ξ for three reheating EoS, $w_\phi = 0, 1/3, 1/2$. For $w_\phi = 0$, the critical coupling $\xi_{\text{cri}} = 5/48$, and for $w_\phi = 1/2$, critical coupling $\xi_{\text{cri}} \approx 4.073$.

$\xi = 3/16$, and in this range, ν_1 lies within $(0.5, 0]$. According to the spectral index given in Eq.(43), spectrum in the range $1/6 < \xi \leq 3/16$ becomes blue-tilted as shown in magenta and brown color for $\xi = (0.18, 3/16)$ respectively in the middle panel of Fig. 2. For $\xi > 3/16$, ν_1 becomes imaginary as is obvious from (44). With the further increase of ξ , the independence of ν_2 makes the slope of the spectrum completely insensitive to the coupling strength in the entire range $\xi > 3/16$ although our numerical analysis shows very slow growth of the amplitude with increasing ξ (see the green and red lines in the middle panel of Fig.2 for $\xi = (1, 4)$ respectively). From the spectral index given in Eq.(43), in the range $\xi \geq 3/16$, the power spectrum behaves as $\rho_{\chi_k}(\eta) \propto k^3$.

- For $1/3 < w_\phi \leq 1$:

Contrary to the previous case for $0 \leq w_\phi < 1/3$, the energy density spectrum for $1/3 < w_\phi \leq 1$, is blue-tilted in the range $0 \leq \xi < 1/6$ as obvious in the right panel of Fig.2 for $\xi = 0$ (blue line), and as ξ exceeds the conformal limit, the spectrum remains blue-tilted up to $\xi = 3/16$ (see the magenta and brown lines in the right panel of Fig.2) like the previous two cases. However, for $\xi > 3/16$, the energy spectrum has some noticeable features. For this case ν_2 should lie within the range $(1/2, \sqrt{3\xi/2})$. Given an EoS $w_\phi > 1/3$, there exists a particular coupling strength say, $\xi_{\text{cri}} = \frac{(9w_\phi+7)(15w_\phi+1)}{48(3w_\phi-1)}$, at which the spectrum becomes perfectly scale-invariant giving $(2 - \nu_2) = 0$ (see Eq.(43)). For $3/16 < \xi < \xi_{\text{cri}}$, spectrum ρ_{χ_k} remains blue-tilted, $(2 - \nu_2) > 0$ and turns into red-tilted or IR divergent, $(2 - \nu_2) < 0$ for $\xi > \xi_{\text{cri}}$. In the right panel of Fig.2, we notice the scale-invariant and red-tilted spectrum for $\xi = (\xi_{\text{cri}}, 6)$ in green and red lines respectively.

All these important characteristics of the energy density spectrum are shown in Fig.2 for three EoS $w_\phi = 0, w_\phi = 1/3$, and $w_\phi = 1/2$ for different ξ values at some point of time during reheating. Variations of spectral tilt with the variation of ξ are believed to leave a discernible imprint on the induced GWs spectrum, which we intend to investigate in the subsequent section.

4. Spectral behavior of “ $\rho_{\chi_k}(\eta)$ ” for varying time :

Here we show for a certain coupling strength how the spectral shape will change over time during the reheating phase. We notice that as we go deep into the reheating phase $\eta \gg \eta_{\text{end}}$, the amplitude of the spectrum gets diminished for a given k -mode as obvious in Fig.3, and this is because of the decaying nature of every mode after horizon reentry during reheating. For the chosen value of coupling strength $\xi = 3$, the blue-tilted nature of the energy density spectra for $w_\phi = 0, 1/3, 1/2$ are also consistent with the expressions given in Eqs. (42) and (43).

D. Defining the Reheating Parameters ($N_{\text{re}}, T_{\text{re}}$) :

In this section we introduce pivotal inflationary parameters namely the inflationary energy scale (H_{end}), the duration of the inflationary period denoted by e-folding number N_* , and define a crucial reheating parameter, namely the *Reheating Temperature* (T_{re}). From the CMB pivot scale, we have $(k_*/a_0) = 0.05\text{Mpc}^{-1}$ where a_0 is the present-day

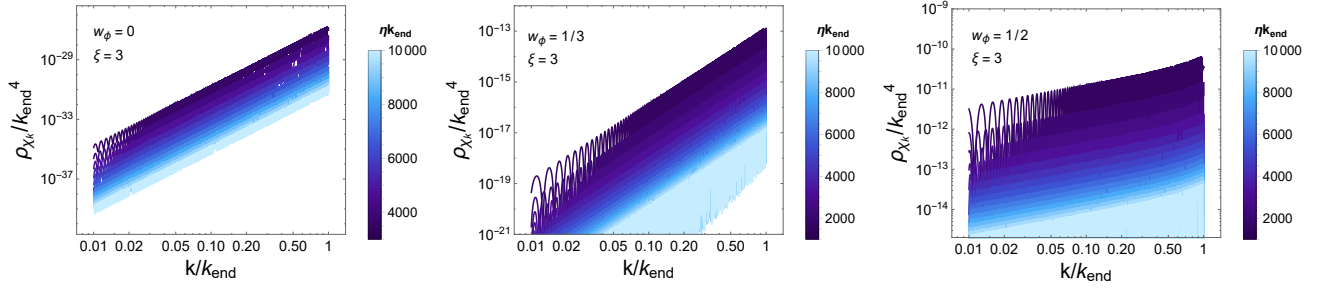


FIG. 3: Figure represents the behavior of dimensionless scalar field energy density spectrum $\rho_{\chi_k}(\eta)/k_{\text{end}}^4$ for three EoS and a specific coupling strength $\xi = 3$ with the variation of dimensionless time-variable ηk_{end} indicated by the color bar where the color gradient is indicating this time-evolution in the post-inflationary phase.

scale factor, and k_{end} denotes the wave number that crosses the Hubble radius at the end of inflation, and connecting these two scales, we express $k_{\text{end}} = k_* e^{N_*}$.

The Planck data imposes constraints on the amplitude of scalar perturbation and tensor-to-scalar ratio, setting them at $A_s = 2.1 \times 10^{-9}$ and $r_{0.05} \leq 0.036$ [41, 91]. With $H_{\text{end}} = \pi M_{\text{pl}} \sqrt{r A_s}/2$, the constraint on r implies $H_{\text{end}} \lesssim 10^{-5} M_{\text{pl}}$, where $M_{\text{pl}} = 1/\sqrt{8\pi G}$ is the reduced Planck mass as mentioned earlier.

Assuming the reheating dynamics are characterized by an average inflaton equation of state w_ϕ , the evolution of the inflaton energy density during this period is described by the simple expression $\rho_\phi = \rho_\phi^{\text{end}} (a_{\text{end}}/a)^{3(1+w_\phi)}$, where $\rho_\phi^{\text{end}} = 3H_{\text{end}}^2 M_{\text{pl}}^2$ is the total inflaton energy density at the end of inflation.

The reheating temperature is conventionally defined at the end of the reheating period, where the radiation energy density equals the inflaton energy density, i.e., $\rho_R(\eta_{\text{re}}) = \rho_\phi(\eta_{\text{re}})$, with η_{re} being the conformal time defined at the end of the reheating period. Employing this condition, the *Reheating Temperature* (T_{re}) can be expressed as [82, 92]

$$T_{\text{re}} = \left(\frac{90 H_{\text{end}}^2 M_{\text{pl}}^2}{\pi^2 g_{\text{re}}} \right)^{1/4} \exp \left[-\frac{3N_{\text{re}}}{4} (1 + w_\phi) \right]. \quad (45)$$

Alternatively, the duration of the reheating period can be expressed as [92, 93]

$$N_{\text{re}} = \frac{1}{3(1 + w_\phi)} \ln \left(\frac{90 H_{\text{end}}^2 M_{\text{pl}}^2}{\pi^2 g_{\text{re}} T_{\text{re}}^4} \right). \quad (46)$$

Here, $g_{\text{re}} = 106.7$ represents the number of relativistic degrees of freedom at the beginning of the radiation epoch.

Assuming negligible entropy production after reheating, leading to the conservation of comoving entropy density ($a^3(\eta \geq \eta_{\text{re}})s = \text{const}$), we can establish a connection between the lowest possible mode re-entering the horizon at the end of reheating and the reheating temperature as

$$(k_{\text{re}}/a_0) \simeq 3.9 \times 10^6 \left(\frac{T_{\text{re}}}{10^{-2} \text{ GeV}} \right) \text{ Mpc}^{-1}. \quad (47)$$

By utilizing Eq. (46), we can define the largest mode that left the horizon at the end of inflation as

$$(k_{\text{end}}/a_0) = \left(\frac{43}{11g_{\text{re}}} \right)^{1/3} \left(\frac{\pi^2 g_{\text{re}}}{90} \right)^\alpha \frac{H_{\text{end}}^{1-2\alpha} T_{\text{re}}^{4\alpha-1} T_0}{M_{\text{pl}}^{2\alpha}}, \quad (48)$$

where $\alpha = 1/3(1 + w_\phi)$ and $T_0 = 2.725 \text{ K}$ is the present-day CMB temperature.

III. PRODUCTION OF GRAVITATIONAL WAVES

In this section, our primary interest is to investigate the effect of the produced scalar fluctuations in the presence of non-minimal coupling as a possible source of anisotropy on gravitational waves. As previously argued, this type of coupling induces instability in the post-inflationary reheating phase. Depending upon the reheating EoS in the

following section we investigate the impact of scalar field *Tachyonic instability* induced anisotropy stress and the associated secondary gravitational waves (SGWs).

The large-scale growth of χ field during de Sitter inflation and post-inflationary phase generates a significant level of anisotropy with an anisotropic stress tensor $\Pi_{ij} \sim \partial_i X \partial_j X$. The perturbed FLRW metric can be written as

$$ds^2 = a^2(\eta) [-d\eta^2 + (\delta_{ij} + h_{ij})dx^i dx^j], \quad (49)$$

where η is the conformal time and h_{ij} is the traceless tensor, i.e. $\partial^i h_{ij} = h_i^i = 0$. Now to find the dynamical equation of tensor perturbation we shall treat ' $h_{ij}(\eta, \mathbf{x})$ ' as a quantum field in an unperturbed FRW background metric, and if we keep up to quadratic order in ' h_{ij} ', the tensor perturbations in the presence of anisotropic stress are governed by the following action [94]

$$S_{GW} = \int dx^4 \sqrt{-g} \left[-\frac{g^{\mu\nu}}{64\pi G} \partial_\mu h_{ij} \partial_\nu h_{ij} + \frac{1}{2} \Pi_{ij} h_{ij} \right], \quad (50)$$

where ' Π_{ij} ' is the anisotropic stress, defined as [94] $\Pi_j^i = T_j^i - p\delta_j^i$. Here ' Π_{ij} ' also satisfies the transverse ($\partial^i \Pi_{ij} = 0$) and traceless ($\Pi_i^i = 0$) conditions. Here Π_{ij} coupled with the tensor-perturbations h_{ij} acting like an external source. From the expression of the stress-energy tensor of a massless scalar field having non-minimal gravity coupling $\xi\chi^2 R$ [71, 72, 95], we write the expression of anisotropic stress tensor as

$$\Pi_{ij} \sim (1 - 2\xi)\partial_i \chi \partial_j \chi - 2\xi\chi\partial_i \partial_j \chi + \xi\chi^2 G_{ij} \quad (51)$$

By varying h_{ij} in action (50), we obtain the equation of motions of h_{ij} [96, 97]

$$h_{ij}''(\eta, \mathbf{x}) + 2\mathcal{H}h_{ij}'(\eta, \mathbf{x}) - \nabla^2 h_{ij}(\eta, \mathbf{x}) = 16\pi G a^2 \left(1 - \frac{a^2 \xi \langle \chi^2 \rangle}{M_{pl}^2} \right)^{-1} \left((1 - 2\xi)\partial_i \chi \partial_j \chi - 2\xi\chi\partial_i \partial_j \chi \right), \quad (52)$$

where the vacuum expectation value of fluctuations square can be expressed in terms of Fourier modes as

$$\langle \chi^2 \rangle = \frac{1}{a^2} \int_{k_{re}}^{k_{end}} \frac{k^3}{2\pi^2} |X_k|^2 dk. \quad (53)$$

For our specific choices of ξ , $a^2 \xi \langle \chi^2 \rangle < M_{pl}^2$ should be always satisfied. Therefore, $\left(1 - a^2 \xi \langle \chi^2 \rangle / M_{pl}^2 \right) \approx 1$ is well justified. Now it is good to write the above Eq(52) in the following fashion [98–102]

$$h_{ij}''(\eta, \mathbf{x}) + 2\mathcal{H}h_{ij}'(\eta, \mathbf{x}) - \nabla^2 h_{ij}(\eta, \mathbf{x}) = \frac{2}{M_{pl}^2} P_{ij}^{lm} T_{lm}(\eta, \mathbf{x}) \quad (54)$$

where $P_{ij}^{lm} = P_i^l P_j^m - P_{ij} P^{lm}/2$ is the transverse traceless projector with $P_{ij} = \delta_{ij} - \partial_i \partial_j / \Delta$ and for massless non-minimally coupled system $T_{lm}(\eta, \mathbf{x}) = (1 - 2\xi)\partial_l \chi \partial_m \chi + (2\xi - \frac{1}{2})g_{lm}(\partial_\alpha \chi \partial^\alpha \chi) + 2\xi(g_{lm} \chi \square \chi - \chi \nabla_l \partial_m \chi) + \xi G_{lm} \chi^2$ [71, 72] represents the spatial part of the stress-energy momentum tensor of the scalar field χ .

Recall that the tensor perturbations $h_{ij}(\eta, \mathbf{x})$ evolving in a Friedmann universe can be decomposed in terms of the Fourier modes, say, $h_{\mathbf{k}}^\lambda(\eta)$, as follows:

$$h_{ij}(\eta, \mathbf{x}) = \sum_{\lambda=(+, \times)} \int \frac{d^3 \mathbf{k}}{(2\pi)^{3/2}} e_{ij}^\lambda(\mathbf{k}) h_{\mathbf{k}}^\lambda(\eta) e^{i\mathbf{k} \cdot \mathbf{x}}, \quad (55)$$

where $e_{ij}^\lambda(\mathbf{k})$ is the polarization tensor corresponding to the mode with wave vector \mathbf{k} and the index λ represents the two types of polarization of the GWs. Note that $e_{ij}^\lambda(\mathbf{k})$ is assumed to be real in the linear polarization basis and implying $h_{-\mathbf{k}}^\lambda(\eta) = h_{\mathbf{k}}^{\lambda*}(\eta)$, and the mode functions $h_{\mathbf{k}}^\lambda(\eta)$ satisfy the following inhomogeneous equation [98, 99, 101]:

$$h_{\mathbf{k}}^{\lambda''} + 2\frac{a'}{a} h_{\mathbf{k}}^{\lambda'} + k^2 h_{\mathbf{k}}^\lambda = \frac{2}{M_{pl}^2} e_{ij}^{\lambda}(\mathbf{k}) P_{ij}^{lm}(\hat{k}) T_{lm}(\mathbf{k}, \eta). \quad (56)$$

For this type of source, we chose the linear polarization basis where both polarization modes contribute equally to the total energy density of the produced gravitational waves (GWs). Henceforth, We drop the polarization index to

simplify the notation and incorporate its information into the tensor power spectrum. The tensor power spectrum is defined as

$$\mathcal{P}_T(k, \eta) = \delta^{(3)}(\mathbf{k} - \mathbf{k}_1) \frac{k^3}{2\pi^2} \sum_{\lambda=+, \times} \langle h_{\mathbf{k}}^\lambda(\eta) h_{\mathbf{k}_1}^{\lambda*}(\eta) \rangle = 4 \frac{k^3}{2\pi^2} |h_{\mathbf{k}}(\eta)|^2 \quad (57)$$

Utilizing the Green's function method, the solution for tensor perturbation can be expressed as[103]

$$h_{\mathbf{k}}(\eta) = h_{\mathbf{k}}^{\text{vac}} + \frac{2e^{ij}(\mathbf{k})}{M_{\text{pl}}^2} \int d\eta_1 \mathcal{G}_k(\eta, \eta_1) \Pi_{ij}^{\text{TT}}(\mathbf{k}, \eta_1). \quad (58)$$

Here $h_{\mathbf{k}}^{\text{vac}}$ is the homogeneous contributions of the tensor fluctuations and $\mathcal{G}_k(\eta, \eta_1)$ is the retarded propagator solving the Eq.(54) with delta function source. In the above Eq.(58) we define $\Pi_{ij}^{\text{TT}}(\mathbf{k}, \eta_1) = P_{ij}^{lm}(\mathbf{k}) T_{lm}(\eta, \mathbf{k})$ with $P_{ij}^{lm}(\mathbf{k})$ and $T_{lm}(\eta, \mathbf{k})$ being the Fourier transformation of the transverse traceless projector and the energy-momentum tensor respectively.

By substituting Eq. (58) into Eq. (57), we derive the secondary production of the tensor power spectrum, which is defined as

$$\mathcal{P}_T^{\text{sec}}(k, \eta) = 4 \frac{k^3}{2\pi^2} \frac{4}{M_{\text{pl}}^4} \int_{\eta_i}^{\eta_f} d\eta_1 \mathcal{G}_k(\eta, \eta_1) \int_{\eta_i}^{\eta_f} d\eta_2 \mathcal{G}_k(\eta, \eta_2) \Pi^2(k, \eta_1, \eta_2). \quad (59)$$

Here, η_i and η_f represent the initial and final times when the source was active to produce the tensor fluctuations. The term Π^2 on the right-hand side is defined as the correlator of the source Π_{ij}^{TT} , given by [104]:

$$\langle 0 | \Pi_{ij}^{\text{TT}}(\mathbf{k}, \eta_1) \Pi_{ij}^{\text{TT}*}(\mathbf{k}_1, \eta_2) | 0 \rangle = \delta^3(\mathbf{k} - \mathbf{k}_1) \Pi^2(k, \eta_1, \eta_2). \quad (60)$$

Utilizing Eq.(4) and promoting it so quantum field $a(t)\chi_k = \hat{a}_{\mathbf{q}} X_{\mathbf{q}}(\eta) + \hat{a}_{-\mathbf{q}}^\dagger X_{\mathbf{q}}^*(\eta)$ [104] we can write the Fourier expression of the source term as

$$\Pi_{ij}^{\text{TT}}(\mathbf{k}, \eta) = \frac{(1 - 4\xi) P_{ij}^{lm}(\hat{k})}{(2\pi)^3 a^2(\eta)} \int d^3q q_l q_m \langle (\hat{a}_{\mathbf{q}} X_{\mathbf{q}}(\eta) + \hat{a}_{-\mathbf{q}}^\dagger X_{\mathbf{q}}^*(\eta)) (\hat{a}_{\mathbf{k}-\mathbf{q}} X_{\mathbf{k}-\mathbf{q}}(\eta) + \hat{a}_{-(\mathbf{k}-\mathbf{q})}^\dagger X_{\mathbf{k}-\mathbf{q}}^*(\eta)) \rangle. \quad (61)$$

The creation ($\hat{a}_{\mathbf{q}}$) and annihilation $\hat{a}_{-\mathbf{q}}^\dagger$ operators which contribute to the expectation value of Eq.(61) are

$$\langle 0 | \hat{a}_{\mathbf{q}} \hat{a}_{\mathbf{k}-\mathbf{q}} \hat{a}_{\mathbf{q}_1}^\dagger \hat{a}_{\mathbf{k}_1-\mathbf{q}_1}^\dagger | 0 \rangle = (2\pi)^6 \left[\delta^{(3)}(\mathbf{k} - \mathbf{q} - \mathbf{q}_1) + \delta^{(3)}(\mathbf{q} - \mathbf{q}_1) \right] \delta^{(3)}(\mathbf{k} - \mathbf{k}_1), \quad (62a)$$

$$\langle 0 | \hat{a}_{\mathbf{q}} \hat{a}_{-(\mathbf{k}-\mathbf{q})}^\dagger \hat{a}_{\mathbf{q}_1} \hat{a}_{-(\mathbf{k}_1-\mathbf{q}_1)}^\dagger | 0 \rangle = (2\pi)^6 \delta^{(3)}(\mathbf{k}) \delta^{(3)}(\mathbf{k}_1 - \mathbf{k}), \quad (62b)$$

where we used the following commutation relation $[\hat{a}_{\mathbf{k}}, \hat{a}_{\mathbf{k}_1}^\dagger] = (2\pi)^3 \delta^{(3)}(\mathbf{k} - \mathbf{k}_1)$. Since the second term Eq.(62b) does not contribute to $\Pi^2(k, \eta, \eta_1)$ due to the finite momenta i.e. $k = k_1 \neq 0$. The only term Eq.(62a) contributes to the final expression of the correlator as

$$\Pi^2(k, \eta_1, \eta_2) = \frac{(1 - 4\xi)^2}{4\pi^2 a^2(\eta_1) a^2(\eta_2)} \int dqq^6 \int d\gamma (1 - \gamma^2)^2 \langle X_{\mathbf{q}}(\eta_1) X_{\mathbf{k}-\mathbf{q}}(\eta_1) X_{\mathbf{q}}^*(\eta_2) X_{\mathbf{k}-\mathbf{q}}^*(\eta_2) \rangle \quad (63)$$

where $\gamma = \hat{k} \cdot \hat{q} = \cos(\theta)$, where θ is the angle between \mathbf{k} and \mathbf{q} . Note that at $\xi = 1/4$ the leading order $\mathcal{O}(1/M_p^2)$ contribution to the energy momentum vanishes, and sub leading $\mathcal{O}(1/M_p^4)$ contribution will contribute. However, we will see that to achieve an appreciable strength of the SGW spectrum, ξ should always remain in the domain greater than unity.

Now utilizing Eq.(63) in Eq.(59) we have found the tensor power spectrum to be

$$\begin{aligned} \mathcal{P}_T^{\text{sec}}(k, \eta) &= \frac{k^3}{2\pi^2} \frac{4(1 - 4\xi)^2}{\pi^2 M_{\text{pl}}^4} \times \int_0^\infty dq q^6 \int_{-1}^1 d\gamma (1 - \gamma^2)^2 \\ &\times \int_{\eta_{\text{end}}}^\eta d\eta_1 \frac{\mathcal{G}_k^{\text{re}}(\eta, \eta_1)}{a^2(\eta_1)} \int_{\eta_{\text{end}}}^\eta d\eta_2 \frac{\mathcal{G}_k^{\text{re}}(\eta, \eta_2)}{a^2(\eta_2)} \langle X_{\mathbf{q}}(\eta_1) X_{\mathbf{k}-\mathbf{q}}(\eta_1) X_{\mathbf{q}}^*(\eta_2) X_{\mathbf{k}-\mathbf{q}}^*(\eta_2) \rangle \end{aligned} \quad (64)$$

Here $\mathcal{P}_T^{\text{sec}}(k, \eta)$ defines the secondary tensor power spectrum during reheating at conformal time η induced due to massless scalar field χ .

A. Evolution of Primordial Tensor Power spectrum during Reheating:

This subsection provides a concise overview of the primary tensor power spectrum and its evolution resulting from quantum fluctuations during inflation. Inflation, a crucial mechanism addressing cosmological challenges such as flatness and horizon problems, offers a well-established framework for generating tensor fluctuations from the quantum vacuum. The tensor power spectrum, characterizing the distribution of gravitational waves across cosmic scales, provides valuable insights into the universe's inflationary phase and subsequent evolution.

Within the context of a simple slow-roll inflationary background, the primary tensor power spectrum resulting from quantum production can be approximated as [82, 105, 106]:

$$\mathcal{P}_T^{\text{pri}}(k, \eta_{\text{end}}) \approx \frac{2}{\pi^2} \left(\frac{H_{\text{end}}}{M_{\text{pl}}} \right)^2 \left(1 + \frac{k^2}{k_{\text{end}}^2} \right) \quad (65)$$

Here, k_{end} represents the highest momentum leaving the horizon at the end of inflation.

Following inflation, the reheating phase converts inflaton energy into radiation, leading to a radiation-dominated universe characterized by the equation of state (w_ϕ) and reheating temperature (T_{re}). The Hubble parameter evolves as $H^2 = H_{\text{end}}^2 (a/a_{\text{end}})^{-3(1+w_\phi)}$, influencing the scale factor's evolution $a(\eta) \approx a_{\text{end}} (\eta/\eta_{\text{end}})^{2/(1+3w_\phi)}$. This results in the evolution of tensor fluctuations $h_{\mathbf{k}}$ during reheating without any source term:

$$h_{\mathbf{k}}''(x) + \frac{4}{1+3w_\phi} \frac{1}{x} h_{\mathbf{k}}'(x) + h_{\mathbf{k}}(x) = 0. \quad (66)$$

Here, we introduce the dimensionless variable $x = k\eta$. The well-known solution to this equation is given by:

$$h_{\mathbf{k}}(x) = \mathcal{C}_1 x^{l(w_\phi)} J_{l(w_\phi)}(x) + \mathcal{C}_2 x^{l(w_\phi)} J_{-l(w_\phi)}(x), \quad (67)$$

where $J_l(x)$ is the Bessel function of order $l(w_\phi) = 3(w_\phi - 1)/2(1 + 3w_\phi)$ and the two integration constants \mathcal{C}_1 and \mathcal{C}_2 contain critical information regarding the origin of tensor fluctuations during inflation. Determining these constants involves satisfying continuity conditions for both tensor fluctuations and their first derivatives at $\eta = \eta_{\text{end}}$. Focusing on modes beyond the Hubble radius at the end of inflation, we can calculate \mathcal{C}_1 and \mathcal{C}_2 in the super-horizon limit ($x_e = k\eta_{\text{end}} \ll 1$). The expressions are as follows:

$$\mathcal{C}_1 = \frac{\pi}{2 \sin(l\pi)} \left(\frac{k}{k_{\text{end}}} \right)^{2(1-l)} \left(\frac{1}{\Gamma(2-l)} + \frac{1}{\Gamma(1-l)} \right) h_{\mathbf{k}}(k, \eta_{\text{end}}), \quad (68)$$

$$\mathcal{C}_2 = \frac{\pi}{2 \sin(l\pi)} \left(\frac{1}{\Gamma(l)} - \frac{1}{\Gamma(1+l)} \left(\frac{k}{k_{\text{end}}} \right)^2 \right) h_{\mathbf{k}}(k, \eta_{\text{end}}) \quad (69)$$

where $h_{\mathbf{k}}(k, \eta_{\text{end}})$ is the amplitude of tensor fluctuation at the inflation end [82, 106]. In the general scenario, the parameter w_ϕ lies within $0 \leq w_\phi \leq 1$, causing $l(w_\phi)$ to take negative values consistently. Given our interest in scales beyond the horizon at the end of inflation (i.e., $k < k_{\text{end}}$, implying $k/k_{\text{end}} < 1$), we assert that \mathcal{C}_2 greatly dominates over \mathcal{C}_1 .

Finally, utilizing Eqs.(67) and (69) in Eq.(57), we obtain the primary GW spectrum at the end of reheating as [106]:

$$\mathcal{P}_T^{\text{pri}}(k, \eta_{\text{re}}) = \frac{\pi^2}{4 \sin^2(l\pi) \Gamma^2(l)} \left(1 - \frac{1}{l} \left(\frac{k}{k_{\text{end}}} \right)^2 \right)^2 \mathcal{P}_T^{\text{pri}}(k, \eta_{\text{end}}). \quad (70)$$

B. Productions of Secondary Tensor Power spectrum during Reheating:

As previously discussed in Section II, the non-minimal coupling can introduce an instability in field dynamics, and that eventually leads to a significant growth of the scalar fluctuation. For higher value of $\xi > 1$, it is evident from the right panel of Fig.1 that for any EoS $0 \leq w_\phi \leq 1$, the effect of this instability is much stronger for large scales ($k < k_{\text{end}}$) than the small scales ($k > k_{\text{end}}$) modes. As a result, we observe the growth of the large-scale modes as depicted in Fig.1, and this growth is prominent exclusively in reheating scenarios where $w_\phi > 1/3$ in larger ξ regimes. On the contrary, for $w_\phi < 1/3$, the growth of the large-scale modes becomes significant in the lower ξ regimes, particularly below the conformal limit $0 \leq \xi < 1/6$, which causes an enhanced energy density spectrum ρ_{χ_k} as shown in the left panel of Fig.2.

The secondary tensor power spectrum $\mathcal{P}_T^{\text{sec}}(k, \eta)$ corresponding to this period is detailed in Eq. (64), where $\mathcal{G}_k^{\text{re}}(\eta, \eta_1)$ represents the Green's function associated with Eq. (54), satisfying the following differential equation [82]

$$\mathcal{G}_k''(\eta, \eta_1) + 2\mathcal{H}\mathcal{G}_k'(\eta, \eta_1) + k^2\mathcal{G}_k(\eta, \eta_1) = \delta(\eta - \eta_1). \quad (71)$$

The Green's function during the reheating epoch is expressed as [82]

$$\mathcal{G}_k^{\text{re}}(\eta, \eta_1) = \Theta(\eta - \eta_1) \frac{\pi\eta^l\eta_1^{1-l}}{2\sin(l\pi)} [J_l(k\eta)J_{-l}(k\eta_1) - J_{-l}(k\eta)J_l(k\eta_1)]. \quad (72)$$

Utilizing Eq. (41) and (72) in Eq. (64), we have obtained the general expressio of the secondary tensor power spectrum due to the massless scalar field χ at the end of the reheating era $\eta = \eta_{\text{re}}$ as follows,

$$\mathcal{P}_T^{\text{sec}}(k, \eta_{\text{re}}) = \frac{2\mathcal{A}^2 H_{\text{end}}^4}{\pi^4 M_{\text{pl}}^4} \left(\frac{k}{k_{\text{end}}}\right)^{4+2\delta-4\nu_2} \left(\int_{x_e}^{x_{\text{re}}} dx_1 x_1^{-\delta} \mathcal{G}_k^{\text{re}}(x_{\text{re}}, x_1) \mathcal{I}(x_1)\right)^2 \mathcal{F}(k), \quad (73)$$

where $\delta(w_\phi) = 4/(1 + 3w_\phi)$. This equation introduces one dimensionless variable: $x = k\eta$ or $x_1 = k\eta_1$. The time integral limits range from $x_e = k\eta_{\text{end}}$ to $x_{\text{re}} = k\eta_{\text{re}}$. The momentum integral part $\mathcal{F}(k)$ is detailed in the Appendix A.

Upon evaluating all the integrals, the resulting secondary tensor power spectrum at the end of reheating for $w_\phi > 1/3$ and $\xi > 3/16$ turns out to be

$$\mathcal{P}_T^{\text{sec}}(k, \eta_{\text{re}}) = \frac{2\mathcal{A}^2 H_{\text{end}}^4}{\pi^4 M_{\text{pl}}^4} \left(\frac{k}{k_{\text{end}}}\right)^{4+2\delta-4\nu_2} \mathcal{I}_t^2(x_{\text{re}}, x_e) \mathcal{F}(k). \quad (74)$$

Here, \mathcal{A} is defined as

$$\mathcal{A} \approx \left(\frac{(1 - 4\xi)^{1/2} \Gamma(\nu_2) \exp(-\pi\tilde{\nu}_1/2)}{4} \left(\frac{2}{3\mu - 1}\right)^{\nu_2} \sqrt{3\mu - 1} \left| \frac{(\pi + i \cosh(\pi\tilde{\nu}_1) \Gamma(1 - i\tilde{\nu}_1) \Gamma(i\tilde{\nu}_1))}{\pi \Gamma(i\tilde{\nu}_1)} \right| \right)^2, \quad (75)$$

whereas the time integral part \mathcal{I}_t is defined as (see the details in Appendix A)

$$\mathcal{I}_t(x_{\text{re}}, x_e) = \int_{x_e}^{x_{\text{re}}} dx_1 x_1^{-\delta} \mathcal{I}(x_1) \mathcal{G}_k^{\text{re}}(x_{\text{re}}, x_1), \quad (76)$$

and

$$\mathcal{F}(k) \simeq \frac{16}{15} \left\{ \frac{1}{6 - 2\nu_2} \left(1 - \left(\frac{k_{\text{min}}}{k}\right)^{6-2\nu_2}\right) + \frac{1}{5 - 4\nu_2} \left(\left(\frac{k_{\text{end}}}{k}\right)^{5-4\nu_2} - 1\right) \right\}. \quad (77)$$

Proceeding in the same way, utilizing the Eq.(42) we obtain the secondary tensor power spectrum for $w_\phi < 1/3$ and $\xi < 3/16$ as

$$\mathcal{P}_T^{\text{sec}}(k, \eta_{\text{re}}) = \frac{2\mathcal{B}^2 H_{\text{end}}^4}{\pi^4 M_{\text{pl}}^4} \left(\frac{k}{k_{\text{end}}}\right)^{4+2\delta-4(\nu_1+\nu_2)} \mathcal{I}_t^2(x_{\text{re}}, x_e) \mathcal{E}(k). \quad (78)$$

where \mathcal{B} is defined as

$$\mathcal{B} \approx \left(\frac{(1 - 4\xi)^{1/2} \Gamma(\nu_1) \Gamma(\nu_2) 2^{\nu_1}}{8\pi} \left(\frac{2}{3\mu - 1}\right)^{\nu_2} \left(\frac{3\mu(1 - 2\nu_1) + 2(\nu_1 - \nu_2)}{\sqrt{3\mu - 1}}\right) \right)^2. \quad (79)$$

Here the expression of the time-integral $\mathcal{I}_t(x_{\text{re}}, x_e)$ will remain unchanged and momentum-integral will be modified as

$$\mathcal{E}(k) \simeq \frac{16}{15} \left\{ \frac{1}{6 - 2(\nu_1 + \nu_2)} \left(1 - \left(\frac{k_{\text{min}}}{k}\right)^{6-2(\nu_1+\nu_2)}\right) + \frac{1}{5 - 4(\nu_1 + \nu_2)} \left(\left(\frac{k_{\text{end}}}{k}\right)^{5-4(\nu_1+\nu_2)} - 1\right) \right\}. \quad (80)$$

Now we shall define the dimensionless energy density of the gravitational waves $\Omega_{\text{gw}}(k)h^2$ for *today* in the following subsection.

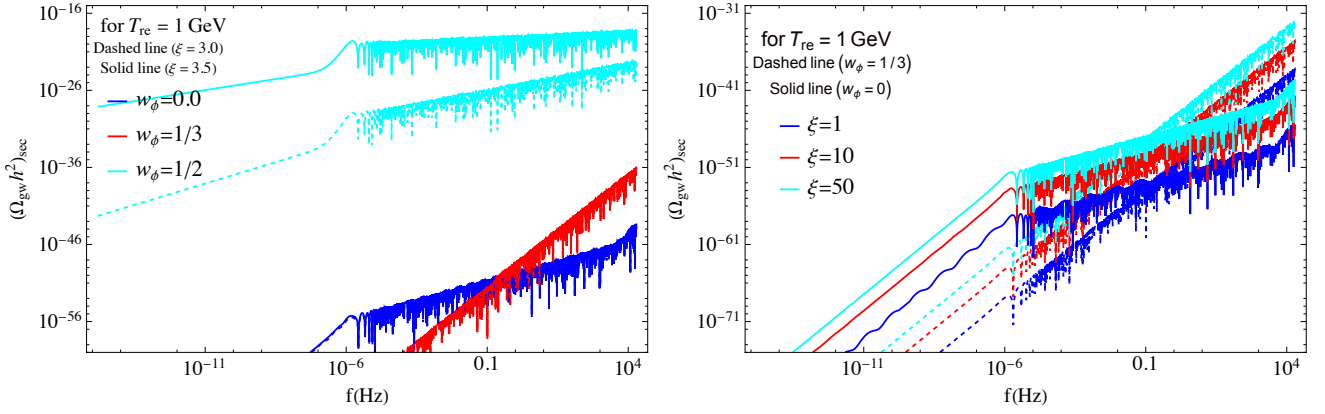


FIG. 4: In this figure, we have shown the present-day dimensionless gravitational waves energy density $(\Omega_{\text{gw}}h^2)_{\text{sec}}$ (induced by the scalar field only) as a function of frequency f (Hz). The left panel illustrates the dependency of the EoS $w_\phi = 0, 1/3$, & $1/2$ for two specific values of the coupling constant $\xi = 3.5$ (indicated by solid lines) and $\xi = 3.0$ (indicated by dashed lines). In the right panel, we have shown how the spectral energy density evolves for the coupling constants $\xi = 1, 10$, & 50 , with fixed EoS values $w_\phi = 0$ (indicated by solid lines) and $w_\phi = 1/3$ (indicated by dashed lines). In both panels, we have considered the reheating temperature of our universe to be $T_{\text{re}} = 1 \text{ GeV}$.

C. GW spectrum for today :

During the reheating and radiation-dominated epochs, perturbation modes progressively re-enter the Hubble radius, producing a stochastic gravitational wave (GW) signal. When produced in the early universe, this GW signal is assumed to possess statistical homogeneity, isotropy, and Gaussianity, inheriting properties from the FLRW universe, whether during inflation or the thermal era.

Due to the weak interaction of gravity with matter, GWs are decoupled from the rest of the universe at the Planck scale. Neglecting interactions with ordinary matter and self-interactions, we assume that sub-Hubble GWs propagate freely in space after their production or re-entry into the Hubble radius. The GW energy density decays with the expansion of the universe, mimicking the behavior of radiation, i.e., $\rho_{\text{gw}} \propto a^{-4}$. Meanwhile, the physical wave number of GWs evolves as k/a . Deep inside the radiation-dominated universe, given the spectrum, the normalized GW energy density parameter at any time η is defined as

$$\Omega_{\text{gw}}(k, \eta) = \frac{\rho_{\text{gw}}(k, \eta)}{\rho_c(\eta)} = \frac{k^2 \mathcal{P}_{\text{T}}^{\text{rad}}(k, \eta)}{12a^2(\eta)H^2(\eta)}. \quad (81)$$

Here, the critical energy density $\rho_c(\eta) = 3H^2(\eta)M_{\text{pl}}^2$, and $M_{\text{pl}} \simeq 2.43 \times 10^{18} \text{ GeV}$ represents the reduced Planck mass. The tensor power spectrum $\mathcal{P}_{\text{T}}^{\text{rad}}(k, \eta)$ during radiation-dominated era can further be expressed in terms of the spectrum at the end of reheating as [82].

$$\mathcal{P}_{\text{T}}^{\text{rad}}(k, \eta) = \left(1 + \frac{k^2}{k_{\text{re}}^2}\right) \frac{\mathcal{P}_{\text{T}}(k, \eta_{\text{re}})}{2k^2\eta^2}. \quad (82)$$

As is well-established, the energy density of gravitational waves (GWs) exhibits a behavior akin to radiation, scaling as $\rho_{\text{gw}} \propto a^{-4}$. Our focus lies on modes that are well within the Hubble radius at a later time, particularly in proximity to the radiation-matter equality epoch during radiation domination. We express the dimensionless energy density parameter $\Omega_{\text{gw}}(k)$ today in terms of $\Omega_{\text{gw}}(k, \eta)$ as follows, as described in [82, 106]:

$$\Omega_{\text{gw}}(k)h^2 = \left(\frac{g_{r,eq}}{g_{r,0}}\right) \left(\frac{g_{s,0}}{g_{s,eq}}\right)^{4/3} \Omega_R h^2 \Omega_{\text{gw}}(k, \eta) \approx \left(\frac{g_{r,0}}{g_{r,eq}}\right)^{1/3} \Omega_R h^2 \Omega_{\text{gw}}(k, \eta). \quad (83)$$

Here, $\Omega_R h^2 = 4.3 \times 10^{-5}$, representing the dimensionless energy density of radiation at the present epoch. $g_{r,eq}$ and $g_{r,0}$ represent the number of relativistic degrees of freedom at radiation-matter equality and in the present era, respectively, whereas $g_{s,eq}$ and $g_{s,0}$ signify the number of such degrees of freedom contributing to entropy at these respective epochs. In our calculation we adopt the values $g_{r,eq} \simeq g_{s,eq} = 106.7$ and $g_{r,0} \simeq g_{s,0} = 3.35$.

a. Primary GWs spectrum today(PGWs): After the reheating epoch, the subsequent era is predominantly characterized by radiation. Now utilizing Eqs (70) and (81) in Eq.(83) we have found that the PGWs *today* can be estimated as [82]

$$\Omega_{\text{gw}}^{\text{pri}}(k)h^2 \simeq 1.12 \cdot 10^{-17} \left(\frac{\Omega_R h^2}{4.3 \times 10^{-5}} \right) \left(\frac{H_{\text{end}}}{10^{-5} M_{\text{pl}}} \right)^2 \times \begin{cases} \mathcal{D}_1 & \text{for } k < k_{\text{re}} \\ \mathcal{D}_2(k/k_{\text{re}})^{n_w} & \text{for } k_{\text{re}} < k < k_{\text{end}} \end{cases}. \quad (84)$$

Here, we introduce the parameter $n_w = 2(3w_\phi - 1)/(1 + 3w_\phi)$, and define $\mathcal{D}_1 = \pi^2 2^{2l}/4 \sin^2(l\pi) \Gamma^2(l) \Gamma^2(1-l) \simeq \mathcal{O}(1)$ and $\mathcal{D}_2 \simeq (\pi^2/2 \sin^2(l\pi) \Gamma^2(l)) \cos^2(-k/k_{\text{re}} + (1-2l)\pi/4) \simeq \mathcal{O}(1)$.

b. Secondary GWs spectrum today(SGWs): Similarly, using Eqs. (74), (78), and (81) in Eq.(83) we have found that the secondary GWs spectrum for the modes $k_* \leq k \leq k_{\text{end}}$ can be estimated as

$$\begin{aligned} \Omega_{\text{gw}}^{\text{sec}}(k)h^2 \simeq & 2.22 \times 10^{-26} \left(\frac{\Omega_R h^2}{4.3 \times 10^{-5}} \right) \left(\frac{H_{\text{end}}}{10^{-5} M_{\text{pl}}} \right)^4 \left(1 + \frac{k^2}{k_{\text{re}}^2} \right) \mathcal{I}_t(k, \eta_{\text{re}}) \\ & \times \begin{cases} \mathcal{B}^2 \left(\frac{k}{k_{\text{end}}} \right)^{4+2\delta-4(\nu_1+\nu_2)} \mathcal{E}(k) & \text{for } w_\phi < 1/3, \xi < 3/16 \\ \mathcal{A}^2 \left(\frac{k}{k_{\text{end}}} \right)^{4+2\delta-4\nu_2} \mathcal{F}(k) & \text{for } w_\phi > 1/3, \xi > 3/16 \end{cases} \end{aligned} \quad (85)$$

In this context, $\mathcal{I}_t(k, \eta_{\text{re}})$ represents the time integral as defined in Eq. (76), while \mathcal{A} and \mathcal{B} denote the constant coefficients consisting of the EoS parameter and coupling strength (w_ϕ, ξ), as outlined in Eq.(75), and (79).

- For $w_\phi > 1/3, \xi > 3/16$: This the region of parameter space, for which the scalar field growth is prominent for the range of scales which has wider detection prospects of a large pool of ongoing and future GW experiments. We consider two distinct regimes to analyze the spectral behavior of secondary gravitational waves: $k \ll k_{\text{re}}$ and $k_{\text{re}} \ll k < k_{\text{end}}$. In the super-horizon limit, the SGW spectrum follows the relation $\Omega_{\text{gw}}^{\text{sec}}(k \ll k_{\text{re}})h^2 \propto f^{4(2-\nu_2)}$. In contrast, in the sub-horizon limit, the spectrum exhibits a behavior of $\Omega_{\text{gw}}^{\text{sec}}(k \gg k_{\text{re}})h^2 \propto f^{6+\delta-4\nu_2}$ (for further details, refer to the Appendix A).

As previously discussed, for an EoS with $w_\phi > 1/3$ and a coupling parameter $\xi > 1/6$, a post-inflationary parametric instability arises in the scalar field χ , and significantly enhances the overall production of the scalar field during the reheating era. On the contrary, in scenarios where $w_\phi \leq 1/3$, no such post-inflationary instability occurs. In Fig. (4), we showed how such growths are imprinted in SGWs depending upon w_ϕ and the coupling parameter ξ . In the left panel, we examine three EoS values: $w_\phi = 0, 1/3$, and $1/2$, with a fixed reheating temperature of $T_{\text{re}} = 1$ GeV. The secondary GW spectrum generically acquires a common factor $\Omega_{\text{gw}}^{\text{sec}}(k)h^2 \propto (k_{\text{end}}/k_{\text{re}})^{\frac{6w_\phi-2}{1+3w_\phi}}$ (see the detailed calculation in appendix A). The factor immediately suggests that for $w_\phi < 1/3$ ($w_\phi > 1/3$), the amplitude of the spectrum is significantly suppressed (enhanced) as $k_{\text{end}}/k_{\text{re}} \gg 1$. This suppression or enhancement can indeed be seen from the left panel of Fig. 4. Detailed calculation further indicates that when $w_\phi \leq 1/3$, the secondary GW production is always overshadowed by the primary production for all scales as far as larger coupling values, $\xi > 3/16$, are concerned. However, for $w_\phi = 1/2$ (i.e., $w_\phi > 1/3$) in the larger coupling regime, the production of SGWs due to the scalar field is significantly enhanced in super-horizon modes, potentially surpassing the primary gravitational wave production.

In the top left panel of Fig. 5, we explore the dependency of the coupling parameter ξ for two different EoS values: $w_\phi = 0$ and $1/3$. As neither of these EoS values induces instability in the system, no growth in the scalar field occurs during the reheating era (see Fig. 1). Consequently, the secondary production of gravitational waves is negligible, and the strength of the gravitational wave spectrum remains considerably lower than that of the primary gravitational waves, even when a very high coupling constant ξ is considered.

To this end, we would like to discuss the generic characteristics of the total GW spectrum (PGWs + SGWs) in terms of the reheating parameters, non-minimal coupling, and the inflationary energy scale. In the top left panel, we show the dependency of the reheating temperature on the GW spectrum, with a fixed equation of state $w_\phi = 3/5$ and a coupling constant $\xi = 2.90$. Evidently, in the intermediate frequency range, the secondary production of GWs can surpass the primary gravitational waves (PGWs). The decreasing temperature turns out

to increase the overall amplitude of the spectrum through the factor $\Omega_{\text{gw}}(k)h^2 \propto T_{\text{re}}^{\frac{8(1-3w_\phi)}{3(1+w_\phi)}} \propto T_{\text{re}}^{-4/3}$ for $k < k_{\text{re}}$, $w_\phi = 3/5$, and $\Omega_{\text{gw}}(k)h^2 \propto T_{\text{re}}^{\frac{4(1-3w_\phi)}{3(1+w_\phi)}} \propto T_{\text{re}}^{-2/3}$ for $k > k_{\text{re}}, w_\phi = 3/5$. Beyond a certain reheating temperature, however, the large-scale spectrum can exceed the present bound on the tensor-to-scalar ratio $r_{0.05} \leq 0.036$ from

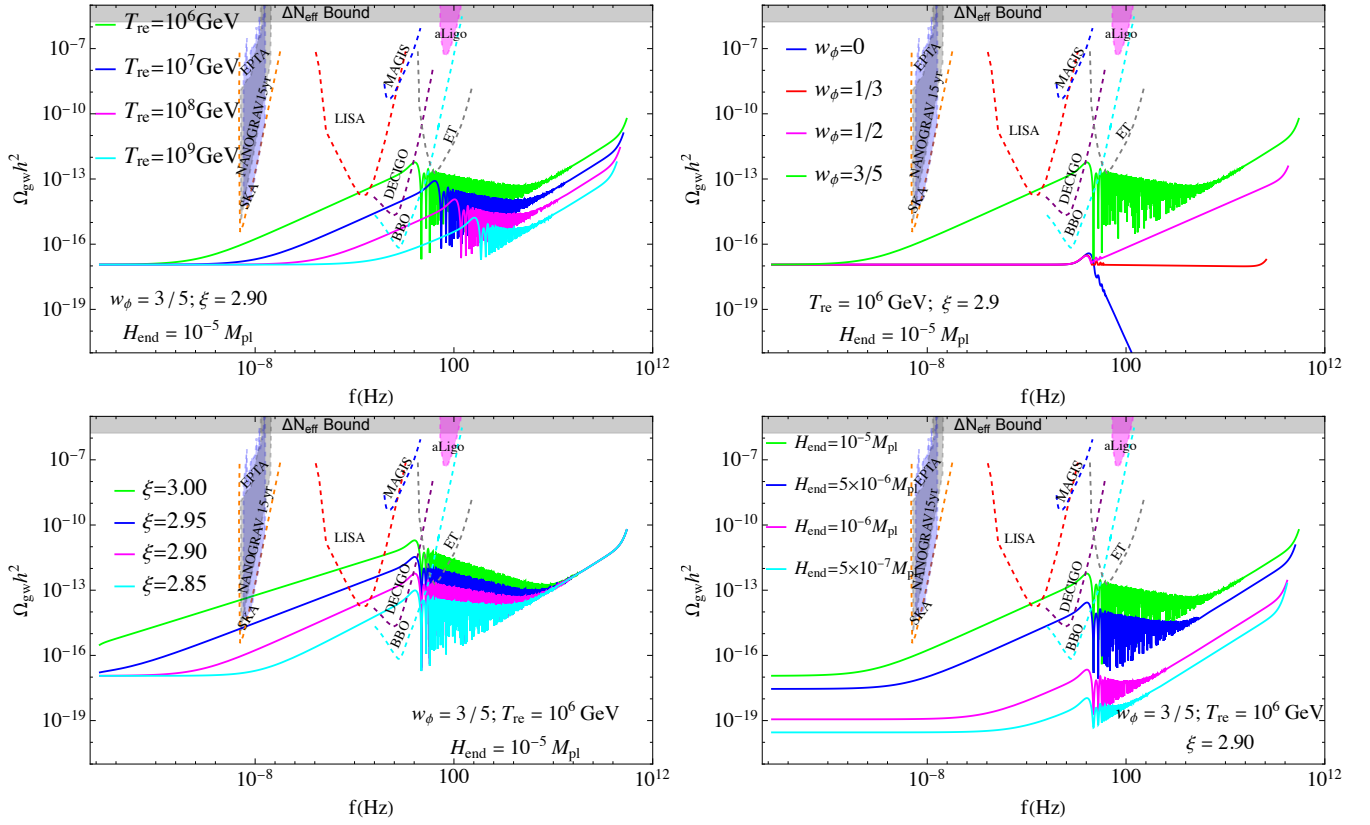


FIG. 5: The figure presents the combined GW spectrum today for different theory parameters. In the top-left panel, we illustrate the dependence of the GW spectrum on the reheating temperature T_{re} for a fixed EoS $w_\phi = 3/5$ with a coupling parameter $\xi = 3.0$. The top-right panel shows the GW spectra for four different EoS values: $w_\phi = 0, 1/3, 1/2,$ and $3/5$, assuming a fixed reheating temperature of $T_{\text{re}} = 10^6$ GeV and a coupling constant $\xi = 2.90$. The bottom-left panel demonstrates the influence of the coupling constant ξ on the GW spectrum, where we assume a fixed reheating scenario with $T_{\text{re}} = 10^6$ GeV and $w_\phi = 3/5$. In all three of these plots, we have adopted the maximal allowed value of the tensor-to-scalar ratio, $r_{0.05} \simeq 0.036$, as constrained by the Planck observations. Finally, in the bottom-right panel, we explore the impact of varying the tensor-to-scalar ratio on the GW spectrum for a fixed reheating scenario with $T_{\text{re}} = 10^6$ GeV, $w_\phi = 3/5$, and $\xi = 2.90$.

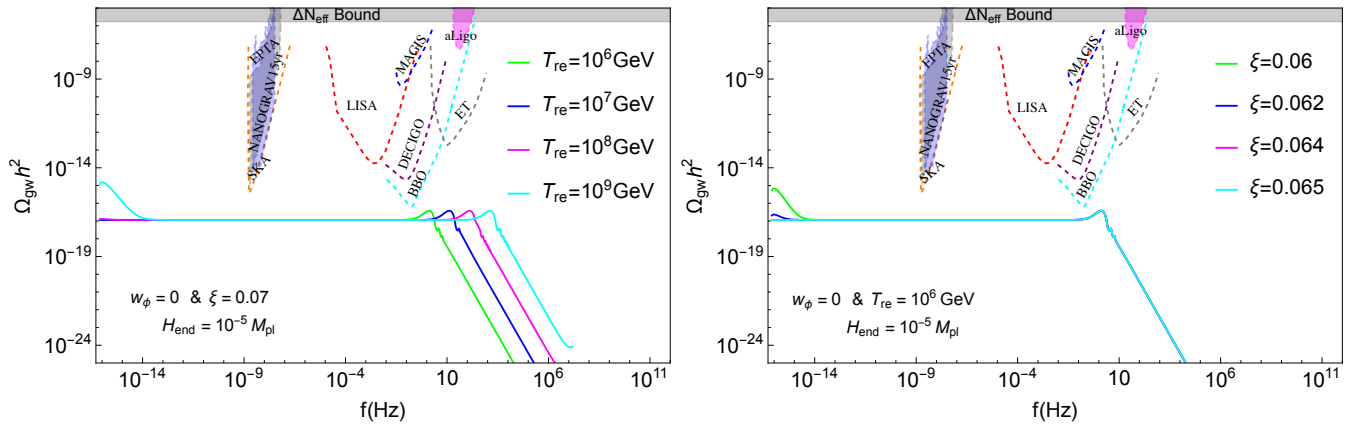


FIG. 6: The figure presents the combined GW spectrum today for different theory parameters. In the left panel of this figure, we show the variation of the GW spectrum for different reheating temperatures with a fixed coupling strength $\xi = 0.07$ and reheating EoS $w_\phi = 0$. In the right panel, we show the dependence of the spectrum on the coupling strength ξ for a fixed reheating temperature $T_{\text{re}} = 10^6$ GeV and EoS $w_\phi = 0$. In these two plots, we have taken the maximal value of the Hubble scale $H_{\text{end}} = 10^{-5} M_{\text{pl}}$.

the recent Planck-2018 results [91], which we discuss in the subsequent section. The spectrum can intersect with future GW sensitivity curves for specific parameter sets, such as LISA, DECIGO, and BBO.

This enhancement of the SGWs with decreasing reheating temperature is effective only for $w_\phi > 1/3$ reheating scenarios due to post-inflationary instability to the scalar field mode. Further lowering the reheating temperature implies an increase in the duration of the reheating period. A longer reheating period implies that the scalar field experiences instability for a more extended period, resulting in greater growth.

Similarly, in the top right panel of Fig.5, we show the evolution of the final GW spectrum for different EoS values, indicated by four different colors. We assume $\xi = 2.90$ and $T_{\text{re}} = 10^6$ GeV. For $w_\phi = 0, 1/3, 1/2$ the PGW dominates the entire spectrum. Although for $w_\phi > 1/3$ and $\xi > 1$, there is instability in field growth (as seen in Fig.1), this growth is insufficient to produce significant GWs to surpass the PGWs generated during inflation due to quantum fluctuations. SGW turns out to dominate only when $w_\phi \geq 3/5$. For example assuming $w_\phi = 3/5$ the spectrum transforms from scale-invariant to blue tilted in the small frequency (large scale) range $f^{8-4\nu_2} = f^{0.41}$, and from blue tilted to red-tilted $f^{6+\delta-4\nu_2} = f^{-0.16}$ for the modes $k > k_{\text{re}}$ (small scale) as indeed observed in green curve. Therefore, for a fixed reheating temperature and coupling constant ($\xi > 1$), there exists a threshold EoS value above which the scalar field growth is sufficient to produce enough SGWs to overtake the PGWs.

In the bottom left panel of Fig. 5, we examine the effect of the coupling constant ξ , with a fixed equation of state $w_\phi = 3/5$ and reheating temperature $T_{\text{re}} = 10^6$ GeV. The results show that increasing the coupling parameter enhances the scalar field's growth due to system instability, thereby enhancing the GW spectrum. The spectral behavior is the same as the previous one with blue tilt in the small frequency (large scale) range $f^{8-4\nu_2}$, and red-tilt $f^{6+\delta-4\nu_2}$ for the modes $k > k_{\text{re}}$ (small scale) as indeed observed in the green curve. We observe that for fixed reheating scenarios (fixed reheating temperature and EoS), there is always a critical value of the coupling constant ξ_{max} , above which the tensor fluctuations at large scales can be overproduced, crossing the present upper bound on the tensor-to-scalar ratio $r_{0.05} \leq 0.036$ set by the Planck collaboration.

In the bottom right panel of Fig. 5, we demonstrate how the gravitational wave (GW) spectrum energy density varies with the inflationary energy scale H_{end} for a fixed reheating temperature of $T_{\text{re}} = 10^6$ GeV and a fixed EoS $w_\phi = 3/5$, with the coupling parameter $\xi = 2.90$. Since the GW spectral energy density is proportional to the fourth power of the inflationary energy scale ($\Omega_{\text{gw}} h^2 \propto H_{\text{end}}^4$), a decrease in H_{end} leads to a corresponding reduction in the amplitude of both primary and secondary GWs due to the factor $(H_{\text{end}}/M_{\text{pl}})$.

For a fixed reheating temperature, lowering the inflationary energy scale by reducing H_{end} leads to a shorter reheating period (see Eq.(46)). The duration of this period is intimately tied to the growth of the scalar field. When the inflationary energy scale H_{end} is reduced, it not only limits the growth of the scalar field during reheating but also affects its initial production during inflation since the scalar field's amplitude depends on the inflationary energy scale. As a result, the overall amplitude of the gravitational wave (GW) spectrum decreases as H_{end} is lowered.

Considering these factors, we find that with $H_{\text{end}} = 10^{-5} M_{\text{pl}}$, $w_\phi = 3/5$, $T_{\text{re}} = 10^6$ GeV, and $\xi = 2.9$, the tensor fluctuations are strong enough to be detected by future sensitivity curves like LISA, DECIGO, and BBO. However, with a lower value like $H_{\text{end}} = 5 \times 10^{-6} M_{\text{pl}}$, the amplitude is suppressed, allowing detection by DECIGO and BBO but not by LISA. For $H_{\text{end}} \leq 10^{-6} M_{\text{pl}}$, the signal is too weak to be detected by upcoming experiments. Therefore, the inflationary energy scale significantly impacts the production of secondary GWs via the scalar field dynamics.

In all figures, at very high-frequency ranges near $f_{\text{end}} = (k_{\text{end}}/2\pi)$, the spectrum follows the $\Omega_{\text{gw}} h^2(f) \propto f^{n_w}$ [82, 106] behavior, which is due to PGWs contributions at these frequencies. At very high frequencies, PGWs dominate over SGWs. As seen in Fig.(3), when the modes re-enter, the scalar field growth is gradually suppressed because the system's instability becomes ineffective once the modes are inside the horizon. The instability-inducing source term $a''/a \sim 1/\eta^2$ decreases over time. Thus, modes deep inside the horizon evolve adiabatically, and the growth time is insufficient to produce significant anisotropy.

- For $0 \leq w_\phi < 1/3$, $\xi < 3/16$: In this region of parameter space the infrared scalar field growth turned out to be relevant around the CMB scales, PLANCK is the only experiment that can place constraints. Likewise the previous case for $w_\phi > 1/3$, we consider here also two distinct regimes of the SGW spectrum, $k \ll k_{\text{re}}$ and $k_{\text{re}} \ll k < k_{\text{end}}$. In the super-horizon limit, the SGW spectrum follows the relation $\Omega_{\text{gw}}^{\text{sec}}(k \ll k_{\text{re}}) h^2 \propto f^{4(2-\nu_1-\nu_2)}$. In contrast, in the sub-horizon limit, the spectrum exhibits a behavior of $\Omega_{\text{gw}}^{\text{sec}}(k \gg k_{\text{re}}) h^2 \propto f^{6+\delta-4(\nu_1+\nu_2)}$ (for detailed calculation see Appendix A). Unlike $w_\phi > 1/3$, for this case the GW spectrum exhibits a sharp enhancement ($(2 - \nu_1 - \nu_2) < 0$) in the long- wavelength modes $k \ll k_{\text{re}}$ particularly for $\xi < 1/6$. We have

presented the dependence of GW spectrum (PGW+SGW) on reheating temperature T_{re} , and the coupling strength ξ for EoS $w_\phi = 0$ in the above Fig. 6. As stated earlier for lower EoS for the modes around CMB pivot scale k_* , the GW spectrum receives significant correction due to tachyonic instability. This makes the spectrum IR divergent with enhanced amplitude, and its value freezes at the end of inflation. Therefore, as the duration of reheating decreases or reheating temperature increases the GW amplitude enhances as $\Omega_{\text{gw}}(k)h^2 \propto (k_{\text{end}}/k_{\text{re}})^{4-2\delta} \propto T_{\text{re}}^{\frac{8(1-3w_\phi)}{3(1+w_\phi)}} \propto T_{\text{re}}^{8/3}$ due to less dilution. For example if $w_\phi = 0$, $\Omega_{\text{gw}}(k)h^2 \propto T_{\text{re}}^{8/3}$ for $w_\phi = 0$ (see left panel of Fig. 6). The right panel depicts the GW spectral behavior for different non-minimal coupling strength ξ with $w_\phi = 0$, $T_{\text{re}} = 10^6$ GeV, and in the regime $k \ll k_{\text{re}}$, it grows as $\Omega_{\text{gw}}(k)h^2 \propto (k/k_{\text{end}})^{8-4(\nu_1+\nu_2)}$. The spectral index $(4(\nu_1 + \nu_2) - 8)$ gradually increases with the decrease of ξ . This is a distinctive feature of the gravitational wave spectrum for $w_\phi < 1/3$, which essentially puts a lower bound on ξ to prevent the overproduction of tensor fluctuations at the CMB scale, and we shall explore these bounds in the next discussion.

c. Constraining the coupling strength ξ from the tensor-to-scalar ratio:

- For $w_\phi > 1/3$: We have discovered that for $w_\phi > 1/3$ reheating scenarios, the scalar field undergoes a tachyonic instability beyond a threshold of the coupling constant ξ , particularly for the super-horizon modes. The significant growth of these super-horizon modes can generate a substantial amount of tensor fluctuations even at Cosmic Microwave Background (CMB) scales. These tensor fluctuations are sufficiently strong to produce a notable tensor-to-scalar ratio at CMB scales. The current observational bound on the tensor-to-scalar ratio at CMB scales is $r_{0.05} \leq 0.036$, as reported by the Planck-2018 observations [91]. By utilizing this bound on $r_{0.05}$, and assuming that all contributions originate from secondary sources (i.e., the scalar fields), we can impose a stringent constraint on the coupling parameter ξ through the following equation

$$r_{0.05} \simeq \frac{2\mathcal{A}^2 H_{\text{end}}^4}{\pi^4 M_{\text{pl}}^4 A_s} \left\{ \frac{1}{2l(\delta-2)} + \frac{1}{4l(1-l)-2l\delta} \right\}^2 \frac{8(1+2\nu_2)}{15(3-\nu_2)(4\nu_2-5)} \times \left(\frac{90H_{\text{end}}^2 M_{\text{pl}}^2}{\pi^2 g_{\text{re}} T_{\text{re}}^4} \right)^{\frac{2(3w_\phi-1)}{3(1+w_\phi)}} \left(\frac{k_*}{k_{\text{end}}} \right)^{4(2-\nu_2)} \leq 0.036 \quad (86)$$

From Eq.(86), it is evident that the reheating dynamics with a specified reheating temperature T_{re} and the average equation of state w_ϕ , has a very sensitive dependence on the maximum coupling strength ξ_{max} to prevent the overproduction of tensor fluctuations at the CMB scale. All the solid curves in Figure (7) depict maximum allowed values of ξ_{max} as a function of w_ϕ for different values of T_{re} . And ξ_{max} represents the value of the coupling constant for a specific set of parameters exceeding which would result in the overproduction of tensor perturbations at the CMB scale, thereby affecting the current bound on the tensor-to-scalar ratio $r_{0.05}$ [91]. For instance, when $w_\phi = 0.5$ and $T_{\text{re}} = 10^{-2}$ GeV, the maximum value of the coupling constant is $\xi_{\text{max}} \simeq 3.73$. On the other hand, if the reheating temperature is $T_{\text{re}} = 10^6$ GeV with the same EoS, the bound turns out to be $\xi_{\text{max}} \simeq 3.99$. The plot shows that ξ_{max} decreases with a reduction in the reheating temperature due to the prolonged duration of the reheating era. During reheating with $w_\phi > 1/3$, the scalar field experiences tachyonic instability; thus, a lower reheating temperature, which implies a longer duration of the reheating period, leads to significant growth in super-horizon modes. We have listed the maximum allowed values of ξ for different reheating temperatures and equation of state in Table I. Evidently, ξ_{max} does not vary much for a wide range of $(T_{\text{re}}, w_\phi, r_{0.05})$. It varies within $\sim (2, 4)$.

- For $w_\phi < 1/3$: In a similar fashion, for $w_\phi < 1/3$, we calculate the tensor-to-scalar ratio at the CMB scale $r_{0.05}$ as

$$r_{0.05} \simeq \frac{2\mathcal{B}^2 H_{\text{end}}^4}{\pi^4 M_{\text{pl}}^4 A_s} \left\{ \frac{1}{2l(\delta-2)} + \frac{1}{4l(1-l)-2l\delta} \right\}^2 \frac{8(1+2(\nu_1+\nu_2))}{15(3-(\nu_1+\nu_2))(4(\nu_1+\nu_2)-5)} \times \left(\frac{90H_{\text{end}}^2 M_{\text{pl}}^2}{\pi^2 g_{\text{re}} T_{\text{re}}^4} \right)^{\frac{2(3w_\phi-1)}{3(1+w_\phi)}} \left(\frac{k_*}{k_{\text{end}}} \right)^{4(2-\nu_1-\nu_2)} \leq 0.036 \quad (87)$$

The negative value of the index $(2 - \nu_1 - \nu_2)$ in the lower the value of $\xi < 1/6$ renders the higher the strength of the GW spectrum for $w_\phi < 1/3$. This fact sets the lower limit of ξ_{min} that satisfies the observational bound on $r_{0.05}$. For instance, for $w_\phi = 0$, we obtain $\xi_{\text{min}} \simeq (0.02036, 0.04179, 0.05935, 0.07394)$, for $w_\phi = 0.1$, we

	T_{re} (GeV)	$w_\phi = 0$	$w_\phi = 1/2$	$w_\phi = 3/5$	$w_\phi = 4/5$	$w_\phi = 99/100$
$r_{0.05} = 0.036$	10^{-2}	0.02036	3.7312	2.7649	2.1056	1.8818
	10^2	0.04179	3.8599	2.9034	2.2611	2.0529
	10^6	0.05935	3.9955	2.9867	2.4342	2.2482
$r_{0.05} = 10^{-4}$	10^{-2}	0.01668	3.7950	2.8136	2.1443	1.9168
	10^2	0.03903	3.9289	2.9569	2.3059	2.095
	10^6	0.05728	4.0691	3.1111	2.4859	2.299

TABLE I: In the above table, we have listed the minimum possible values ξ_{\min} for $w_\phi = 0$ and maximum possible values ξ_{\max} for higher reheating EoS $w_\phi = 1/2, 3/5, 4/5, 0.99$ for different reheating temperatures T_{re} . The lower bound ξ_{\min} for $w_\phi = 0$ is derived from Eq. (87) and the upper bound ξ_{\max} for higher EoS $w_\phi > 1/3$ is derived from Eq. (86) to avoid the overproduction of tensor perturbations at the CMB scale. Based on recent observations from Planck, We consider the upper bound on the tensor-to-scalar ratio to be $r_{0.05} = 0.036$. We also show the slight variation of both ξ_{\min} and ξ_{\max} with tensor-to-scalar ratio by considering another value at the CMB scale $r_{0.05} = 10^{-4}$.

obtain $\xi_{\min} \simeq (5.4 \times 10^{-4}, 0.01569, 0.02916, 0.04119)$ for $T_{\text{re}} = (10^{-2}, 10^2, 10^6, 10^{10})$ GeV respectively and for $w_\phi = 0.2$, we obtain $\xi_{\min} \simeq (3.35 \times 10^{-3}, 0.01104)$ for $T_{\text{re}} = (10^6, 10^{10})$ GeV respectively. For $w_\phi = 0.2$, no lower limit exists for the temperatures $T_{\text{re}} = (10^{-2}, 10^2)$ GeV. Interestingly, as one gradually approaches $w_\phi = 1/3$, the system becomes unconstrained meaning no lower and upper boundary of coupling strength ξ exists to prevent overproduction for any reheating temperature in a specified range. As an example, for $w_\phi = 0.33$ and $\xi = 0$, we find $r_{0.05} = (2.88 \times 10^{-11}, 3.46 \times 10^{-11}, 4.17 \times 10^{-11}, 5 \times 10^{-11})$ for $T_{\text{re}} = (10^{-2}, 10^2, 10^6, 10^{10})$ GeV respectively.

d. *Constraining the coupling strength ξ and reheating dynamics through ΔN_{eff} :* The total radiation density around the time of decoupling influences the cosmic microwave background (CMB). At that epoch, neutrinos comprised a significant fraction of the radiative energy, but additional radiation (such as dark radiation or primordial gravitational waves) may also impact the CMB spectrum. In this context, treating the χ field as dark radiation significantly affects the CMB spectra through the extra radiation component. The effective number of neutrino species, N_{eff} , which represents the energy density stored in relativistic components (radiation), is defined as

$$\rho_{\text{ra}} = \rho_\gamma + \rho_\nu + \rho_x = \left[1 + \frac{7}{8} \left(\frac{4}{11} \right)^{4/3} N_{\text{eff}} \right] \rho_\gamma \quad (88)$$

where ρ_γ , ρ_ν , and ρ_x are the energy densities of photons, neutrinos, and extra radiation components (massless scalar field (ρ_χ) or primordial gravitational waves (ρ_{gw})), respectively. From Eq. (88), the excess radiation component can be defined as:

$$\rho_\chi = \frac{7}{8} \left(\frac{4}{11} \right)^{4/3} \rho_\gamma \Delta N_{\text{eff}} \quad (89)$$

where $\Delta N_{\text{eff}} = N_{\text{eff}} - N_\nu$ represents the extra relativistic degrees of freedom. Here, ρ_x includes both dark radiation ρ_χ and primordial gravitational waves ρ_{gw} , with N_{eff} being the observed total relativistic degrees of freedom and $N_\nu = 3.044$ representing the standard model neutrino degrees of freedom [107–111].

To determine the contribution of the dark radiation, specifically the massless scalar field χ , we can express Eq. (89) as:

$$\rho_\chi = \frac{1}{2\pi^2 a^4} \int_{k_{\text{re}}}^{k_{\text{end}}} \frac{dk}{k} k^4 |\beta_k|^2 = \frac{7}{8} \left(\frac{4}{11} \right)^{4/3} \rho_\gamma \Delta N_\chi \quad (90)$$

where ΔN_χ is the extra relativistic degree of freedom due to the dark radiation field χ . This computation of ρ_χ in different ξ ranges is detailed in the Appendix B. For the sake of convenience, we introduce a new dimensionless variable $\Omega_\chi(\eta_{\text{re}}) = \rho_\chi(\eta_{\text{re}})/\rho_c(\eta_{\text{re}})$, where $\rho_c(\eta_{\text{re}}) = 3H_{\text{re}}^2 M_{\text{pl}}^2$ is the background energy density at the end of reheating. As both the background energy density (ρ_c) and the massless scalar field (considered as dark radiation ρ_χ) goes as a^{-4}

due the background expansion, the fractional energy density $\Omega_\chi(\eta > \eta_{\text{re}} < \eta_{\text{eq}})$ remain conserved during radiation dominated era. The present-day fractional energy density of the χ field can be expressed as

$$\Omega_\chi h^2 \simeq \left(\frac{g_{r,0}}{g_{r,eq}} \right)^{1/3} \Omega_{\text{R}} h^2 \Omega_\chi(\eta_{\text{re}}) \quad (91)$$

where $\Omega_{\text{R}} h^2 \simeq 4.3 \times 10^{-5}$ [91] denotes the dimensionless energy density of radiation at the current epoch. Here, $g_{r,eq}$ and $g_{r,0}$ represent the number of relativistic degrees of freedom at the epochs of radiation-matter equality and the present day, respectively. By expressing Eq. (90) in terms of this dimensionless variable, we obtain

$$\Omega_\chi h^2 = \frac{7}{8} \left(\frac{4}{11} \right)^{4/3} \Omega_\gamma h^2 \Delta N_\chi \simeq 1.6 \times 10^{-6} \left(\frac{\Delta N_\chi}{0.284} \right) \quad (92)$$

where $\Omega_\gamma h^2 = 2.47 \times 10^{-5}$ is the present-day photon energy density [91]. The latest Planck data with Baryon Acoustic Oscillation (BAO) predicts $\Delta N_{\text{eff}} \leq 0.284$ (within 2σ range) [91]. Using this bound as an upper limit, we can further constrain the coupling parameter ξ through Eq.(92).

We find that coupling strength ξ is further constrained through ΔN_{eff} for $w_\phi > 1/3$. In Fig.(7), we have plotted the upper limit of the coupling parameter ξ_{max} as a function of the average equation of state $w_\phi > 1/3$ for five different reheating temperatures. Lowering the reheating temperature for a fixed EoS tightens the constraint on ξ . For example, if the EoS is $w_\phi = 0.5$ and the reheating temperature of our universe is $T_{\text{re}} = 10^{-2}$ GeV, then to satisfy the current ΔN_{eff} bound, the maximum allowed value of the coupling parameter is $\xi_{\text{max}} \simeq 4.02$. Note this is greater than the bound we obtained from the tensor-to-ratio ($\xi_{\text{max}} \simeq 3.73$) discussed before. On the other hand, if the reheating temperature is $T_{\text{re}} = 10^6$ GeV with the same EoS, the bound is $\xi_{\text{max}} \simeq 4.99$, which is again higher than the bound from the tensor to ratio ($\xi_{\text{max}} \simeq 3.99$) discussed before.

It is to be noted that combining constraints from the tensor-to-scalar ratio and from ΔN_{eff} yields significant insights. In the lower reheating temperature case as one reduces the equation state the tensor to scalar ratio tends (solid lines) to provide stronger constraints on ξ_{max} than the ΔN_{eff} , and ΔN_{eff} leads to the maximum possible value of equation state w_ϕ (set by dashed lines). For instance, with $w_\phi = 0.6$ and a reheating temperature of $T_{\text{re}} = 10^{-2}$ GeV, the ΔN_{eff} constraint predicts a maximum allowable value of the coupling constant $\xi_{\text{max}} \simeq 0.205$. In contrast, under the same reheating parameters, the tensor-to-scalar ratio constraint allows a higher upper bound for the coupling constant, $\xi_{\text{max}} \simeq 2.765$. Therefore, we get an allowed region of ξ bounded by solid and dashed lines which satisfy both the constraints. This is indeed the case for red, blue, and magenta curves as depicted in the left panel of Fig.7 for $T_{\text{re}} = (10^{-2}, 10^2, 10^6)$ GeV accordingly. However, with the higher temperature, the constraint from PLANCK on tensor to scalar ratio becomes increasingly important and tends to prove the entire bound on ξ . This indeed can be observed for cyan and brown curves with $T_{\text{re}} = (10^{14}, 10^{10})$ GeV respectively.

Unlike $w_\phi > 1/3$, for $w_\phi < 1/3$, we don't get any new constrain on ξ through ΔN_{eff} bound. As discussed earlier, for $w_\phi < 1/3$, as enhancement effect is important in the range $\xi < 1/6$, we find the lower limit of coupling $\xi_{\text{min}} < \xi_{\text{cri}} < 1/6$ satisfying the tensor-to-scalar ratio bound $r_{0.05} \leq 0.036$. The energy spectrum remains blue-tilted in the entire range $\xi > \xi_{\text{cri}}$. For example, for $\xi = 0$, exploiting the Equations (90)-(92) we obtain for $w_\phi = (0, 0.1, 0.2)$, $\Delta N_{\text{eff}} = (2.88 \times 10^{-13}, 7 \times 10^{-13}, 1.77 \times 10^{-12})$ for a wide range of reheating temperatures $T_{\text{re}} = (10^{-2} - 10^{10})$ GeV (Detail computations of ρ_χ for $w_\phi < 1/3$ are given in Appendix B.). These values are far below the maximum limit $\Delta N_{\text{eff}} \leq 0.284$ for the lowest possible value of $\xi = 0$ meaning no lower limit can be imposed on ξ through ΔN_{eff} for $w_\phi < 1/3$. If we choose $\xi > \xi_{\text{cri}}$, although the energy spectrum is blue-tilted, the secondary GW energy strength is too weak to overtake the primary strength around k_{end} (see Fig.4). Therefore, in this regime, the PGW contribution always dominates the total GW energy density $\Omega_{\text{gw}} h^2$.

Similarly, primordial gravitational waves (PGWs) with frequencies $\geq 10^{-15}$ Hz may contribute significantly to the radiation density of the Universe during the decoupling of the cosmic microwave background (CMB). It can also be treated as an extra relativistic degree of freedom symbolized as ΔN_{gw} . Hence, we can similarly express it as [82, 112]

$$\Omega_{\text{gw}} h^2 = \frac{7}{8} \left(\frac{4}{11} \right)^{4/3} \Omega_\gamma h^2 \Delta N_{\text{gw}} \simeq 1.6 \times 10^{-6} \left(\frac{\Delta N_{\text{gw}}}{0.284} \right) \quad (93)$$

where $\Omega_{\text{gw}} h^2$ is the present-day dimensionless energy density of the gravitational waves produced in the early universe and it is defined as

$$\Omega_{\text{gw}} h^2 = \int_{k_{\text{min}}}^{k_{\text{end}}} \frac{dk}{k} \Omega_{\text{gw}}(k) h_0^2 \quad (94)$$

here $\Omega_{\text{gw}}(k) h^2$ is the total contributions from both primary and secondary gravitational waves. To this end, we should point out that the GW is a secondary contribution

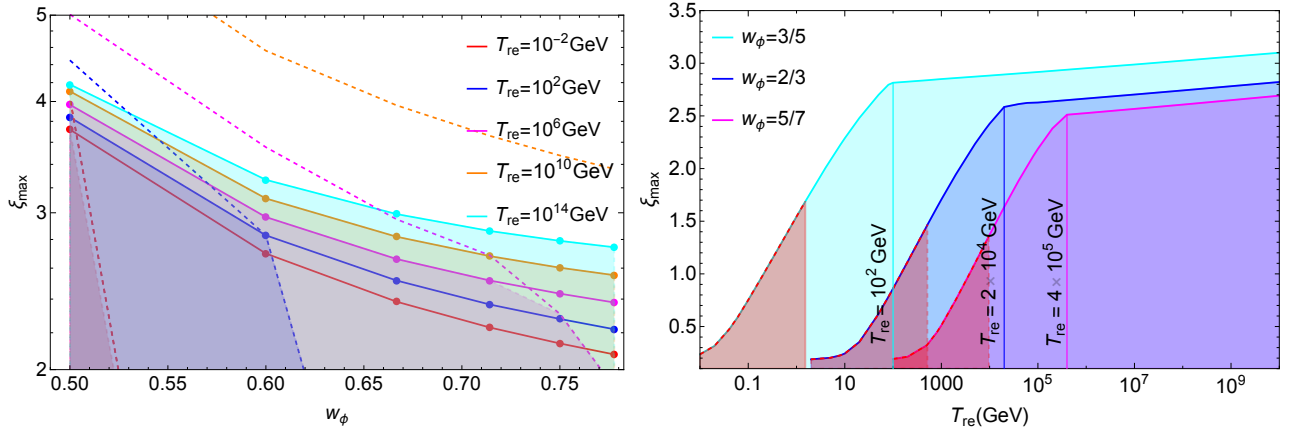


FIG. 7: In the left panel, we present the maximum allowed values of the coupling constant, ξ_{\max} , as a function of w_ϕ . The colored dashed lines represent ξ_{\max} values calculated from the ΔN_{eff} bound (see Eq. (92)). In contrast, the solid colored lines indicate the limit derived from the tensor-to-scalar ratio (see Eq. (86)). Different colors represent different T_{re} values. By combining both limits, we identify a common region allowed under both bounds, represented by the shaded areas corresponding to each color. In the right panel, we plot ξ_{\max} as a function of T_{re} for three discrete values of the equation of state: $w_\phi = 3/5$ (cyan), $w_\phi = 2/3$ (blue), and $w_\phi = 5/7$ (magenta). Combining both constraints, this plot shows the common allowed region, free from the ΔN_{eff} and the tensor-to-scalar ratio bounds. The three vertical lines labeled by specific T_{re} values divided the shaded regions into two. Above this temperature, the tensor-to-scalar ratio imposes a stricter constraint on the coupling parameter ξ compared to the ΔN_{eff} bound. Three red-shaded regions indicate that these reheating temperatures are not allowed for the specified set of w_ϕ values as it violates ΔN_{eff} bound at high frequency near k_{end} primarily sourced by PGWs.

Assuming the present-day photon density parameter is $\Omega_\gamma h^2 \simeq 2.47 \times 10^{-5}$, a combination of the latest Planck-2018 and Baryon Acoustic Oscillation (BAO) data predicts $\Delta N_{\text{eff}} \simeq 0.284$ (within a 2σ range) [91]. Consequently, this prediction sets an upper limit on primordial gravitational waves, such that $\Omega_{\text{gw}} h^2 < 1.6 \times 10^{-6}$ [113]. Using this result, we derive the following inequality [82, 113, 114]

$$\Omega_{\text{gw}} h^2 \leq 1.6 \times 10^{-6} \left(\frac{\Delta N_{\text{gw}}}{0.284} \right) \quad (95)$$

The constraint presented in Eq. (95) imposes a constraints on the reheating temperature;

$$T_{\min} \geq \left(\frac{90 H_{\text{end}}^2 M_{\text{pl}}^2}{\pi^2 g_{\text{re}}} \right)^{1/4} \beta^{\frac{3(1+w_\phi)}{4(3w_\phi-1)}} \left(\frac{0.284}{\Delta N_{\text{gw}}} \right)^{\frac{3(1+w_\phi)}{4(3w_\phi-1)}} \quad (96)$$

Here T_{\min} is the lowest possible reheating temperature to ensure the overproduction of the extra relativistic degree of freedom due to the PGWs. In the above we defined $\beta = 1.43 \times 10^{-11} \mathcal{D}_2(H_{\text{end}}/10^{-5} M_{\text{pl}})^2 / (n_w)$. It is crucial to emphasize that this lower bound on the reheating temperature applies exclusively to the equation of state $w_\phi > 1/3$.

Using Eq. (96), we have generated a parameter space plot of T_{\min} as a function of the average equation of state (w_ϕ) in Fig. (8), showing the minimum permissible reheating temperature as a function of w_ϕ . In this figure, the blue lines correspond to $r_{0.05} = 0.036$, and the magenta lines to $r_{0.05} = 10^{-4}$. Solid lines represent $\Delta N_{\text{eff}} = 0.284$, while dashed lines correspond to $\Delta N_{\text{eff}} = 0.50$. The shaded regions indicate areas excluded due to the overproduction of gravitational waves at high frequencies. The gray shaded region at the bottom excludes reheating temperatures lower than the BBN bound, i.e., $T_{\text{re}}^{\text{BBN}} \simeq 10^{-2}$ GeV. While considering a stiff equation of state ($w_\phi > 1/3$), this bound must be taken into account. In all our plots, we have ensured that this bound is respected to avoid the overproduction of gravitational waves from primary quantum fluctuations during inflation.

e. Constraining Reheating Dynamics and Coupling Parameters ξ via Future Gravitational Wave Experiments:

As depicted in Fig. (5), for an appropriate set of reheating parameters and coupling constant ξ , the production of secondary gravitational waves (SGWs) by the scalar field is significant enough to pass through the sensitivity curves of several forthcoming gravitational wave (GW) detectors, including LISA, DECIGO, BBO, ET, and others. This observation suggests that future GW detectors could probe non-minimal coupling and associated dynamics in the early universe, potentially placing stringent constraints on the coupling parameter ξ and the reheating dynamics. In this section, we point out the parameter space in which these detectors are expected to explore these dynamics.

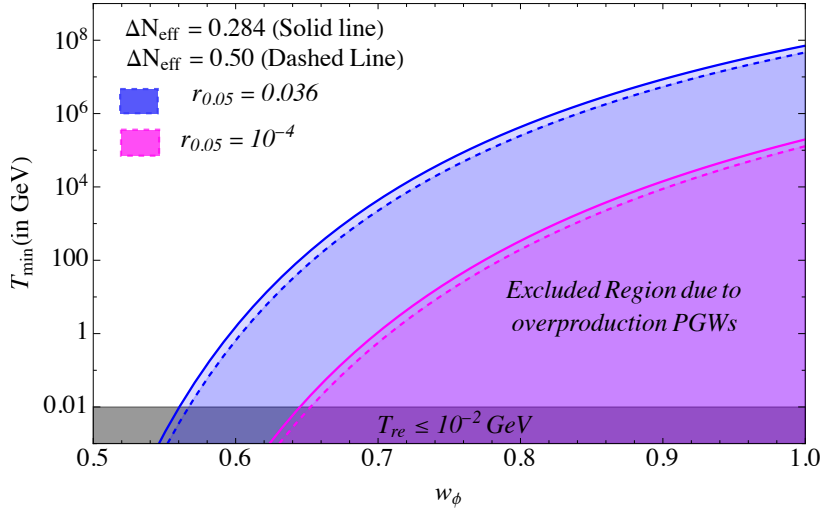


FIG. 8: The figure above shows the minimum allowed reheating temperature T_{\min} (in GeV) as a function of w_ϕ . The blue lines correspond to $r_{0.05} = 0.036$, while the magenta lines represent $r_{0.05} = 10^{-4}$. The solid lines indicate $\Delta N_{\text{eff}} = 0.284$, and the dashed lines indicate $\Delta N_{\text{eff}} = 0.50$. The shaded regions in color mark areas were excluded due to the overproduction of primary gravitational waves at the high-frequency end $f = f_{\text{end}}(k_e/2\pi)$. The gray region at the bottom is excluded due to the minimum reheating temperature required by Big Bang Nucleosynthesis (BBN), which is about $T_{\text{re}} \simeq 10^{-2}$ GeV.

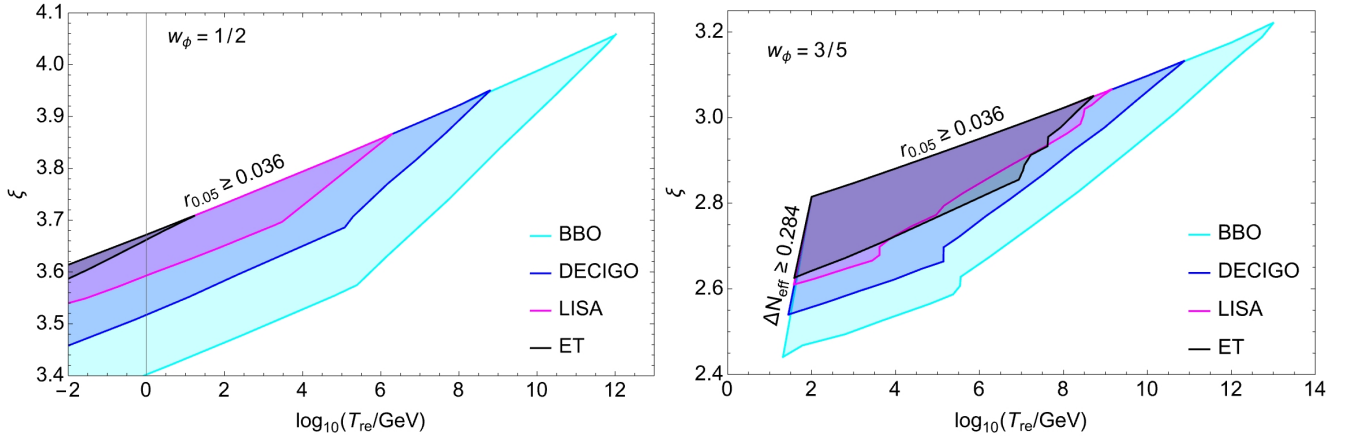


FIG. 9: In the figure above, we present the estimated parameter space of the coupling constant ξ versus the reheating temperature T_{re} for two different equations of state (EoS): $w_\phi = 1/2$, and $w_\phi = 3/5$. These estimates can be tested by future gravitational wave (GW) detectors, including LISA (magenta), DECIGO (blue), BBO (cyan), and ET (gray). Within this parameter space, the signal generated by the scalar field χ can be detected by these GW experiments. In both plots, the upper bound comes from the tensor to scalar ratio at the CMB scale where in the right panel at a lower temperature the ΔN_{eff} puts a stronger constraint on the coupling parameter ξ .

Focusing on future GW experiments such as LISA, DECIGO, BBO, and ET, we utilize the proposed sensitivity curves to estimate the parameter ranges for ξ and the reheating temperature T_{re} for two different equations of state, $w_\phi = 1/2$ and $w_\phi = 3/5$, as shown in Fig. (9). The shaded regions indicate the parameter space where the signal produced by the scalar field is expected to be detectable by these experiments, provided ξ falls within the specified range for a given reheating temperature and equation of state. Notably, the upper bound on ξ remains the same for all experiments, despite differing sensitivity thresholds. This is because the upper limit on ξ is determined by the tensor-to-scalar ratio constraint by PLANCK and the ΔN_{eff} bound (as illustrated in Fig. (7)). Consequently, for values of ξ exceeding a certain threshold, the signal, although potentially detectable, is excluded due to the overproduction of tensor fluctuations and additional relativistic degrees of freedom.

In the right panel of Fig. (9), we observe that when the reheating temperature is relatively low and the scalar field is considered as dark radiation, ΔN_{eff} imposes stricter constraints on ξ , as discussed earlier. Conversely, in the case of $w_\phi = 0.5$ (see in the left panel of Fig.(9)), the tensor-to-scalar ratio constraint is more restrictive than the

ΔN_{eff} constraint. For all the plots the lower boundary is fixed by the lowest values of the gravitational wave strength (sensitivity line) that a particular experiment could measure.

IV. CONCLUSION

Over the past two decades, significant progress has been made in observational cosmology, enhancing our understanding of the universe and its evolutionary trajectories. However, the reheating epoch, a critical phase in cosmic history, remains poorly understood due to the lack of direct observational evidence. Reheating is a localized phenomenon, and information about its dynamics is obscured as the Standard Model (SM) plasma reaches local thermal equilibrium. Understanding how the universe achieves this thermal equilibrium is crucial for comprehending the physics of the early universe. Generally, this thermal bath is produced when the inflaton decays into SM particles, though the exact mechanisms of particle production at this stage are far from complete understanding.

In this study, we investigate the production of a massless scalar field in the presence of a $\xi R\chi^2$ coupling during both inflation and reheating. We found that for $\xi < 1/6$ and $w_\phi < 1/3$, the infrared instability leads to significant growth of the scalar field both during and after inflation. Such growth turns out to be maximal for $\xi = 0$. It potentially violates the PLANCK bound on r through its secondary GW production, thereby setting a tight constraint on the minimum value of ξ . On the contrary, for $\xi > 1/6$, and $w_\phi > 1/3$ the infrared modes of the scalar field grow due to post-inflationary instability, and such instability grows with increasing ξ . Therefore, in this case, the associated induced gravitational waves put a tight constraint on the maximum value of ξ .

To obtain the constraint on ξ , we consider the observational bounds on the effective number of degrees of freedom ΔN_{eff} at the time of BBN and PLANCK's upper limit on tensor to scalar ratio $r_{0.05}$ at the pivot scale (k_*/a_0) = 0.05 Mpc⁻¹. The scalar field generated due to infrared instability can be treated as a possible candidate for dark radiation which contributes to ΔN_{eff} . On the other hand, associated secondary GW can affect both ΔN_{eff} and in estimating the energy scale of inflation through r . Except for a few reheating parameters ($w_\phi > 1/3$, N_{re} , T_{re}), we have found a contrasting prediction of maximum coupling strength ξ_{max} made by these two observations as illustrated in Fig.(7). In the higher reheating temperature regime, we find stronger constraints from the tensor-to-scalar ratio bound that shrinks the maximum allowed region of ξ for given reheating parameters. Combining the latest Planck-2018 data of both $r_{0.05} < 0.036$ and $\Delta N_{\text{eff}} \simeq 0.284$ for $w_\phi \geq 1/2$, we find that there exists an upper limit on $\xi < \xi_{\text{max}} (\simeq 4)$, and hence arbitrarily large values of ξ are hardly acceptable. Likewise, for $w_\phi = 0$, we find that there exists a lower limit on $\xi > \xi_{\text{min}} (\simeq 0.02)$, and hence vanishing non-minimal coupling is excluded. Furthermore, we found distinctive gravitational wave spectrum for different parameters which could be detectable by future GW detectors, allowing for more robust constraints on the coupling parameters and reheating dynamics in the near future GW experiments. Towards the end, given the constraints from all the observations from PLANCK, we derived the region of parameter space in (T_{re}, ξ) plane which can be probed by future experiments such as BBO, DECIGO, LISA, and ET, particularly for stiff inflaton equation of state.

V. ACKNOWLEDGMENTS

AC would like to thank the Ministry of Human Resource Development, Government of India (GoI), for financial assistance. SM gratefully acknowledges the financial support provided by the Council of Scientific and Industrial Research (CSIR), Ministry of Science and Technology, Government of India (GoI), through the Senior Research Fellowship (File No. 09/731(0192)/2021-EMR-I). DM wishes to acknowledge support from the Science and Engineering Research Board (SERB), Department of Science and Technology (DST), Government of India (GoI), through the Core Research Grant CRG/2020/003664.

Appendix A: Computing the Secondary Tensor power spectrum:

As we are mainly interested in the higher post-inflationary EoS regime, $w_\phi > 1/3$, so, we shall first share a detailed calculation of the tensor power spectrum during reheating for a generalized power law type matter power spectrum in stiff EoS regime $w_\phi > 1/3$. The computation of the tensor power spectrum for $w_\phi < 1/3$ will follow the same procedure.

1. For $w_\phi > 1/3$:

For $w_\phi > 1/3$ and $\xi > 3/16$, combining Eqs. (41) and (43) we can write the matter power spectrum in terms of the rescaled field X_k for long-wavelength modes as follows.

$$\mathcal{P}_X(k, \eta) = \frac{k^3}{2\pi^2} \left| X_k^{\text{long}}(k, \eta) \right|^2 = \frac{\mathcal{A}_3}{\pi^2} k_{\text{end}}^2 \mathcal{I}(k, \eta) \left(\frac{k}{k_{\text{end}}} \right)^{2(1-\nu_2)} \quad (\text{A1})$$

In the above equation, \mathcal{A}_3 is a constant part depending on the initial parameters as given in (B3) and $\mathcal{I} = \cos^2(k\eta)$ is the time-dependent part of the matter power spectrum.

Now we can write the tensor power spectrum in terms of the matter power spectrum as

$$\mathcal{P}_T^{\text{sec}}(k, \eta_{\text{re}}) = \frac{8(1-4\xi)^2}{M_{\text{pl}}^4} \left(\int_{x_e}^{x_{\text{re}}} dx_1 \frac{\mathcal{G}_k^{\text{re}}(x_{\text{re}}, x_1)}{a^2(x_1)} \right)^2 \times \int_{k_{\text{min}}}^{k_{\text{end}}} \frac{dq}{k} \int_{-1}^1 d\gamma (1-\gamma^2)^2 \frac{(q/k)^3 \mathcal{P}_X(q, \eta_1) \mathcal{P}_X(|\mathbf{k}-\mathbf{q}|, \eta_1)}{|1-q/k|^3} \quad (\text{A2})$$

Now using Eq.(A1) in the above Eq.(A2) we get the following form.

$$\begin{aligned} \mathcal{P}_T^{\text{sec}}(k, \eta_{\text{re}}) &= \frac{8(1-4\xi)^2 \mathcal{A}_3^2 k_{\text{end}}^4}{\pi^4 M_{\text{pl}}^4} \left(\int_{x_e}^{x_{\text{re}}} dx_1 \frac{\mathcal{G}_k^{\text{re}}(x_{\text{re}}, x_1)}{a^2(x_1)} \mathcal{I}(x_1) \right)^2 \\ &\quad \times \int_{k_{\text{min}}}^{k_{\text{end}}} \frac{dq}{k} \int_{-1}^1 d\gamma (1-\gamma^2)^2 \frac{(q/k)^3 (q/k_{\text{end}})^{2(1-\nu_2)} (|\mathbf{k}-\mathbf{q}|/k_{\text{end}})^{2(1-\nu_2)}}{|1-q/k|^3} \end{aligned} \quad (\text{A3})$$

During the reheating era, the scale factor can be approximately written as $a^2(\eta) \approx a_{\text{end}}^2(x/x_e)^\delta$, we recall that $\delta(w_\phi) = 4/(1+3w_\phi)$. We obtain the following expression by substituting this approximate form of the scale factor to the above Eq.(A3).

$$\begin{aligned} \mathcal{P}_T^{\text{sec}}(k, \eta_{\text{re}}) &= \frac{8(1-4\xi)^2 \mathcal{A}_3^2 H_{\text{end}}^4}{\pi^4 M_{\text{pl}}^4} \left(\frac{k}{k_{\text{end}}} \right)^{4+2\delta-4\nu_2} \left(\int_{x_e}^{x_{\text{re}}} dx_1 x_1^{-\delta} \mathcal{G}_k^{\text{re}}(x_{\text{re}}, x_1) \mathcal{I}(x_1) \right)^2 \\ &\quad \times \int_{k_{\text{min}}}^{k_{\text{end}}} \frac{dq}{k} \int_{-1}^1 d\gamma (1-\gamma^2)^2 (q/k)^{5-2\nu_2} (|1-q/k|)^{-(1+2\nu_2)} \\ &= \frac{8(1-4\xi)^2 \mathcal{A}_3^2 H_{\text{end}}^4}{\pi^4 M_{\text{pl}}^4} \left(\frac{k}{k_{\text{end}}} \right)^{4+2\delta-4\nu_2} \underbrace{\left(\int_{x_e}^{x_{\text{re}}} dx_1 x_1^{-\delta} \mathcal{G}_k^{\text{re}}(x_{\text{re}}, x_1) \mathcal{I}(x_1) \right)^2}_{\text{Time Integral}} \mathcal{F}(k) \end{aligned} \quad (\text{A4})$$

where we define $\mathcal{F}(k)$ as

$$\mathcal{F}(k) = \int_{u_{\text{min}}}^{u_{\text{max}}} du \int_{-1}^1 d\gamma (1-\gamma^2)^2 u^{5-2\nu_2} (1+u^2-2u\gamma)^{-(\nu_2+1/2)} \quad (\text{A5})$$

a. Computation of $\mathcal{F}(k)$:

Here we define another variable $u = q/k$. In order to perform the momentum integral, we have to break it into two separate limits, i.e. $u_{\text{min}} \leq u < 1$ and $1 < u \leq u_{\text{max}}$, where $u_{\text{min}} = k_{\text{min}}/k$ and $u_{\text{max}} = k_{\text{end}}/k$ where k_{min} represents the largest observable scale as of today(CMB scale, k_*) and k_{end} represent the largest mode that leaves the horizon at the end of inflation.

Now in the following range $u_{\text{min}} \leq u < 1$ the above integral (A5) boils down to

$$\mathcal{F}_1 \simeq \int_{u_{\text{min}}}^1 du u^{5-2\nu_2} \int_{-1}^1 d\gamma (1-\gamma^2)^2 = \frac{16}{15(6-2\nu_2)} \left\{ 1 - \left(\frac{k_{\text{min}}}{k} \right)^{6-2\nu_2} \right\} \quad (\text{A6})$$

where we have used $(1+u^2-2\gamma u) \simeq 1$. On the other hand for $1 < u \leq u_{\text{max}}$ range the above integral Eq.(A5) boils down to the following one.

$$\mathcal{F}_2 \simeq \int_1^{u_{\text{max}}} du \int_{-1}^1 d\gamma (1-\gamma^2)^2 u^{5-2\nu_2} u^{-(2\nu_2+1)} = \frac{16}{15(5-4\nu_2)} \left\{ \left(\frac{k_{\text{end}}}{k} \right)^{5-4\nu_2} - 1 \right\}$$

$$= \frac{16}{15(5-4\nu_2)} \left(\frac{k_{\text{end}}}{k}\right)^{5-4\nu_2} \left\{ 1 - \left(\frac{k}{k_{\text{end}}}\right)^{5-4\nu_2} \right\} \quad (\text{A7})$$

where we have used $(1+u^2-2\gamma u) \simeq u^2$.

Now combining Eq.(A6) and Eq.(A7) we get

$$\mathcal{F}(k) = (\mathcal{F}_1 + \mathcal{F}_2) \simeq \frac{16}{15} \left\{ \frac{1}{6-2\nu_2} \left(1 - \left(\frac{k_{\text{min}}}{k}\right)^{6-2\nu_2} \right) + \frac{1}{5-4\nu_2} \left(\left(\frac{k_{\text{end}}}{k}\right)^{5-4\nu_2} - 1 \right) \right\} \quad (\text{A8})$$

b. Simplification of the Time Integral :

During reheating, the Green's function of Eq.(54) is

$$\mathcal{G}_k^{\text{re}}(x, x_1) = \frac{\pi x^l x_1^{1-l}}{2 \sin(l\pi)} (J_l(x) J_{-l}(x_1) - J_{-l}(x) J_l(x_1)) \quad (\text{A9})$$

We recall again $l(w_\phi) = 3(w_\phi - 1)/2(1 + 3w_\phi)$. Now using Eq.(A9) we are going to perform the time integral part of Eq.(A4)

$$\begin{aligned} \mathcal{I}_t(x_{\text{re}}, x_e) &= \int_{x_e}^{x_{\text{re}}} dx_1 x_1^{-\delta} \mathcal{I}(x_1) \mathcal{G}_k^{\text{re}}(x_{\text{re}}, x_1) = \frac{\pi}{2 \sin(l\pi)} \frac{x_{\text{re}}^l x_1^{2-2l-\delta}}{2^{1+l}} \left(-x_1^{2l} J_{-l}(x_{\text{re}}) \Gamma \left[1 - \frac{\delta}{2} \right] \right. \\ &\quad \left. \text{HypergeometricPFQRegularized} \left[\left\{ 1 - \frac{\delta}{2} \right\}, \left\{ 1+l, 2 - \frac{\delta}{2} \right\}, -\frac{x_1^2}{4} \right] \right. \\ &\quad \left. + 4^l J_l(x_{\text{re}}) \Gamma \left[1 - l - \frac{\delta}{2} \right] \text{HypergeometricPFQRegularized} \left[\left\{ 1 - l - \frac{\delta}{2} \right\}, \left\{ 1-l, 2-l - \frac{\delta}{2} \right\}, -\frac{x_1^2}{4} \right] \right) \Big|_{x_e}^{x_{\text{re}}} \quad (\text{A10}) \end{aligned}$$

$$\mathcal{I}_t(x_{\text{re}}, x_e) = (\mathcal{I}_t(x_{\text{re}}, x_{\text{re}}) - \mathcal{I}_t(x_{\text{re}}, x_e)) \simeq \mathcal{I}_t(x_{\text{re}}, x_{\text{re}}) \quad (\text{A11})$$

For the sub-horizon limit i.e.

$$\begin{aligned} \mathcal{I}_t(x_{\text{re}}, x_e) &\simeq -\frac{\pi}{2 \sin(l\pi)} \frac{2^{1-l-\delta} \pi}{\Gamma(l+\delta/2) \Gamma(\delta/2)} x_{\text{re}}^l [\csc(\pi\delta/2) J_{-l}(x_{\text{re}}) - \csc[\pi(2l+\delta)/2] J_l(x_{\text{re}})] \\ &\simeq -\frac{2^{1-l-\delta} \pi \Gamma(1-l) \Gamma(l)}{2\Gamma(l+\delta/2) \Gamma(\delta/2)} x_{\text{re}}^l \sqrt{\frac{2}{\pi x_{\text{re}}}} \{ \csc(\pi\delta/2) \cos[x_{\text{re}} - \pi(1-2l)/4] - \csc[\pi(2l+\delta)/2] \cos[x_{\text{re}} - \pi(1+2l)/4] \} \\ &\simeq -\frac{2^{1-l-\delta} \pi \Gamma(1-l) \Gamma(l)}{2\Gamma(l+\delta/2) \Gamma(\delta/2)} x_{\text{re}}^l \sqrt{\frac{2}{\pi x_{\text{re}}}} \quad (\text{A12}) \end{aligned}$$

Plugging the above Eq.(A12) into the Eq.(A4) we have the following expression.

$$\lim_{k \gg k_{\text{re}}} \mathcal{P}_{\text{T}}^{\text{sec}}(k, \eta_{\text{re}}) \simeq \frac{2(1-4\xi)^2 \mathcal{A}_3^2 H_{\text{end}}^4}{\pi^4 M_{\text{pl}}^4} \frac{2^{1-2l-2\delta} \pi \Gamma^2(1-l) \Gamma^2(l)}{\Gamma^2(l+\frac{\delta}{2}) \Gamma^2(\frac{\delta}{2})} \frac{8(1+2\nu_2)}{15(3-\nu_2)(4\nu_2-5)} \left(\frac{k_{\text{re}}}{k_{\text{end}}}\right)^\delta \left(\frac{k}{k_{\text{end}}}\right)^{4+\delta-4\nu_2} \quad (\text{A13})$$

Similarly for the super-horizon limit i.e. $x_{\text{re}} \ll 1$ limit, the above integral boils down to the simplified form below.

$$\lim_{k \ll k_{\text{re}}} \mathcal{I}_t(x_{\text{re}}, x_e) \simeq x_{\text{re}}^{2-\delta} \left\{ \frac{1}{2l(\delta-2)} + \frac{1}{4l(1-l)-2l\delta} \right\} \quad (\text{A14})$$

Now utilizing this expression in Eq.(A4) we obtain the tensor power spectrum at the super-horizon scale behaving as

$$\begin{aligned} \lim_{k \ll k_{\text{re}}} \mathcal{P}_{\text{T}}^{\text{sec}}(k, \eta_{\text{re}}) &\simeq \frac{2(1-4\xi)^2 \mathcal{A}_3^2 H_{\text{end}}^4}{\pi^4 M_{\text{pl}}^4} \left\{ \frac{1}{2l(\delta-2)} + \frac{1}{4l(1-l)-2l\delta} \right\}^2 \mathcal{F}(k) \left(\frac{k_{\text{end}}}{k_{\text{re}}}\right)^{4-2\delta} \left(\frac{k}{k_{\text{end}}}\right)^{4(2-\nu_2)} \\ &\simeq \frac{2(1-4\xi)^2 \mathcal{A}_3^2 H_{\text{end}}^4}{\pi^4 M_{\text{pl}}^4} \left\{ \frac{1}{2l(\delta-2)} + \frac{1}{4l(1-l)-2l\delta} \right\}^2 \frac{8(1+2\nu_2)}{15(3-\nu_2)(4\nu_2-5)} \left(\frac{k_{\text{end}}}{k_{\text{re}}}\right)^{4-2\delta} \left(\frac{k}{k_{\text{end}}}\right)^{4(2-\nu_2)} \quad (\text{A15}) \end{aligned}$$

a. GWs spectral behaviour for to extreme limit $k \ll k_{\text{re}}$ and $k \gg k_{\text{re}}$: During the radiation-dominated era, the spectral energy density can be written as

$$\Omega_{\text{gw}}(k, \eta) = \frac{\rho_{\text{gw}}(k, \eta)}{\rho_c(\eta)} = \frac{1}{12} \frac{k^2 \mathcal{P}_{\text{T}}^{\text{rad}}(k, \eta)}{a^2(\eta) H^2(\eta)} \quad (\text{A16})$$

where $\mathcal{P}_{\text{T}}^{\text{rad}}(k, \eta)$ is the tensor power spectrum during radiation dominated era and it can be written in terms of $\mathcal{P}_{\text{T}}(k, \eta_{\text{re}})$ as

$$\mathcal{P}_{\text{T}}^{\text{rad}}(k, \eta) = \left(1 + \frac{k^2}{k_{\text{re}}^2}\right) \frac{\mathcal{P}_{\text{T}}(k, \eta_{\text{re}})}{2k^2 \eta^2} \quad (\text{A17})$$

Now utilizing Eq.(A17) and (A15) in Eq.(A16) we obtain the GW spectrum behaving in super-horizon limit as

$$\lim_{k \ll k_{\text{re}}} \Omega_{\text{gw}}(k, \eta) \simeq \frac{2(1-4\xi)^2 \mathcal{A}_3^2 H_{\text{end}}^4}{24\pi^4 M_{\text{pl}}^4} \left\{ \frac{1}{2l(\delta-2)} + \frac{1}{4l(1-l)-2l\delta} \right\}^2 \frac{8(1+2\nu_2)}{15(3-\nu_2)(4\nu_2-5)} \left(\frac{k_{\text{end}}}{k_{\text{re}}}\right)^{4-2\delta} \left(\frac{k}{k_{\text{end}}}\right)^{2(4-2\nu_2)} \quad (\text{A18})$$

Similarly, for sub-horizon modes, using Eq.(A13) and (A17) in Eq.(A16), the GW spectral energy density can be written as

$$\lim_{k \gg k_{\text{re}}} \Omega_{\text{gw}}(k, \eta) \simeq \frac{2(1-4\xi)^2 \mathcal{A}_3^2 H_{\text{end}}^4}{24\pi^4 M_{\text{pl}}^4} \frac{2^{1-2l-2\delta} \pi \Gamma^2(1-l) \Gamma^2(l)}{\Gamma^2(l+\frac{\delta}{2}) \Gamma^2(\frac{\delta}{2})} \frac{8(1+2\nu_2)}{15(3-\nu_2)(4\nu_2-5)} \left(\frac{k_{\text{end}}}{k_{\text{re}}}\right)^{2-\delta} \left(\frac{k}{k_{\text{end}}}\right)^{6+\delta-4\nu_2} \quad (\text{A19})$$

2. For $w_\phi < 1/3$:

It is already discussed in Section II, for $w_\phi < 1/3$, system experiences greater enhancement in long-wavelength regime in the range $\xi < 1/6$. Combining Eqs. (31) and (42) we obtain the expression of the field power spectrum as

$$\mathcal{P}_X(k, \eta) = \frac{k^3}{2\pi^2} \left| X_k^{\text{long}}(k, \eta) \right|^2 = \frac{\mathcal{A}_1}{\pi^2} k_{\text{end}}^2 \mathcal{I}(k, \eta) \left(\frac{k}{k_{\text{end}}}\right)^{2(1-\nu_1-\nu_2)} \quad (\text{A20})$$

In the above equation, \mathcal{A}_1 is a constant part depending on the initial parameters as given in (B1) and $\mathcal{I} = \cos^2(k\eta)$ is the time-dependent part of the matter power spectrum as it was for $w_\phi > 1/3$. Subject to this field power spectrum, following the same steps as followed in the previous case, we obtain the secondary tensor power spectrum as

$$\begin{aligned} \mathcal{P}_{\text{T}}^{\text{sec}}(k, \eta_{\text{re}}) &= \frac{8(1-4\xi)^2 \mathcal{A}_1^2 k_{\text{end}}^4}{\pi^4 M_{\text{pl}}^4} \left(\int_{x_c}^{x_{\text{re}}} dx_1 \frac{\mathcal{G}_k^{\text{re}}(x_{\text{re}}, x_1)}{a^2(x_1)} \mathcal{I}(x_1) \right)^2 \\ &\times \int_{k_{\text{min}}}^{k_{\text{end}}} \frac{dq}{k} \int_{-1}^1 d\gamma (1-\gamma^2)^2 \frac{(q/k)^3 (q/k_{\text{end}})^{2(1-\nu_1-\nu_2)} (|\mathbf{k}-\mathbf{q}|/k_{\text{end}})^{2(1-\nu_1-\nu_2)}}{|1-q/k|^3} \end{aligned} \quad (\text{A21})$$

Comparing Eqs. (A3) and (A21), apart from the time-independent amplitude part (\mathcal{A}_1 and \mathcal{A}_3), we notice the only difference in the index of (q/k_{end}) and $(|\mathbf{k}-\mathbf{q}|/k_{\text{end}})$ ratios. This fact confirms that the substitution of $(\nu_1 + \nu_2)$ in place of ν_2 will essentially reproduce all the results up to Eq.(A19) for $w_\phi < 1/3$ in a similar fashion. Simplification of the following time-integral in (A21) gives the same expression as in (A10). Following the same procedure, the above momentum-integral is simplified as

$$\mathcal{E}(k) \simeq \frac{16}{15} \left\{ \frac{1}{6-2(\nu_1+\nu_2)} \left(1 - \left(\frac{k_{\text{min}}}{k}\right)^{6-2(\nu_1+\nu_2)}\right) + \frac{1}{5-4(\nu_1+\nu_2)} \left(\left(\frac{k_{\text{end}}}{k}\right)^{5-4(\nu_1+\nu_2)} - 1 \right) \right\} \quad (\text{A22})$$

Having followed the same methodology as outlined in the previous case for $w_\phi > 1/3$, we finally reach the GW spectrums in both super-horizon and sub-horizon limits as follows:

a. *GW spectrum in super-horizon* ($k \ll k_{\text{re}}$) *limit*: Likewise (A18), we compute the GW energy density spectrum for super-horizon modes, $k \ll k_{\text{re}}$ as

$$\begin{aligned} \lim_{k \ll k_{\text{re}}} \Omega_{\text{gw}}(k, \eta) &\simeq \frac{2(1-4\xi)^2 \mathcal{A}_1^2 H_{\text{end}}^4}{24\pi^4 M_{\text{pl}}^4} \left\{ \frac{1}{2l(\delta-2)} + \frac{1}{4l(1-l)-2l\delta} \right\}^2 \\ &\times \frac{8(1+2(\nu_1+\nu_2))}{15(3-(\nu_1+\nu_2))(4(\nu_1+\nu_2)-5)} \left(\frac{k_{\text{end}}}{k_{\text{re}}} \right)^{4-2\delta} \left(\frac{k}{k_{\text{end}}} \right)^{2(4-2(\nu_1+\nu_2))} \end{aligned} \quad (\text{A23})$$

b. *GW spectrum in sub-horizon* ($k \gg k_{\text{re}}$) *limit*: Likewise (A19), we compute the GW energy density spectrum for sub-horizon modes, $k \gg k_{\text{re}}$ as

$$\begin{aligned} \lim_{k \gg k_{\text{re}}} \Omega_{\text{gw}}(k, \eta) &\simeq \frac{2(1-4\xi)^2 \mathcal{A}_1^2 H_{\text{end}}^4}{24\pi^4 M_{\text{pl}}^4} \frac{2^{1-2l-2\delta} \pi \Gamma^2(1-l) \Gamma^2(l)}{\Gamma^2(l+\frac{\delta}{2}) \Gamma^2(\frac{\delta}{2})} \\ &\times \frac{8(1+2(\nu_1+\nu_2))}{15(3-(\nu_1+\nu_2))(4(\nu_1+\nu_2)-5)} \left(\frac{k_{\text{end}}}{k_{\text{re}}} \right)^{2-\delta} \left(\frac{k}{k_{\text{end}}} \right)^{6+\delta-4(\nu_1+\nu_2)} \end{aligned} \quad (\text{A24})$$

Appendix B: Energy density of Massless scalar field χ as a dark radiation component for $0 \leq w_\phi \leq 1$:

In this section, employing the Eq.(90) with the knowledge of β_k as calculated in Section II, we shall calculate the energy density of the dark radiation component in different ranges of ξ values for $0 \leq w_\phi \leq 1$.

For $1/3 \leq w_\phi \leq 1$:

1. For $0 \leq \xi < 3/16$

In the given range $0 \leq \xi < 3/16$, the total energy density at the reheating end is computed to be

$$\begin{aligned} \rho_\chi \left(\frac{a}{a_{\text{end}}} \right)^4 &= \frac{\mathcal{A}_1 H_{\text{end}}^4}{2\pi^2} \int_{k_{\text{re}}/k_{\text{end}}}^1 d(k/k_{\text{end}}) (k/k_{\text{end}})^{3-2(\nu_1+\nu_2)} \\ \Rightarrow \rho_\chi &\approx \frac{\mathcal{A}_1 H_{\text{end}}^4}{4\pi^2 (2-(\nu_1+\nu_2))} \exp(-4N_{\text{re}}) \end{aligned} \quad (\text{B1})$$

where $\mathcal{A}_1 = \left(\frac{\Gamma(\nu_1)\Gamma(\nu_2)2^{\nu_1}}{8\pi} \left(\frac{2}{3\mu-1} \right)^{\nu_2} \left(\frac{3\mu(1-2\nu_1)+2(\nu_1-\nu_2)}{\sqrt{3\mu-1}} \right) \right)^2$. For $w_\phi > 1/3$, in this specified range of ξ , we always have $(4-2(\nu_1+\nu_2)) > 0$. So, the maximum contribution to energy is coming from k_{end} . This property of the blue-tilted spectrum is used to reach the final expression of ρ_χ^{com} in Eq.(B1).

2. For $\xi = 3/16$:

Likewise the previous case, the total energy density at the reheating end for $\xi = 3/16$ is evaluated to be

$$\rho_\chi \approx \frac{\mathcal{A}_2 H_{\text{end}}^4}{4\pi^2 (2-\nu_2)} \exp(-4N_{\text{re}}) \quad (\text{B2})$$

where $\mathcal{A}_2 = \left(\frac{\Gamma(\nu_2)}{2} \left(\frac{2}{3\mu-1} \right)^{\nu_2} \left| \frac{3\mu-2\nu_2}{4\sqrt{3\mu-1}} + \frac{i\sqrt{3\mu-1}}{\pi} \right| \right)^2$

3. For $\xi > 3/16$:

In this range, the existence of the critical coupling strength ξ_{cri} (a function of w_ϕ , $\xi_{\text{cri}} = \frac{(9w_\phi+7)(15w_\phi+1)}{48(3w_\phi-1)}$) of the field energy density spectrum, $\rho_{\chi k}$ or $k^4|\beta_k|^2$, distinguishes two regions with a junction that is at $\xi = \xi_{\text{cri}}$.

a. For $3/16 < \xi < \xi_{\text{cri}}$:

For $3/16 < \xi < \xi_{\text{cri}}$, the energy spectrum being blue-tilted again satisfies the same expressions of reheating parameters as in the range $0 \leq \xi \leq 3/16$. The total energy density at the reheating end is computed as

$$\rho_\chi \approx \frac{\mathcal{A}_3 H_{\text{end}}^4}{4\pi^2 (2 - \nu_2)} \exp(-4N_{\text{re}}) \quad (\text{B3})$$

where $\mathcal{A}_3 \approx \left(\frac{\Gamma(\nu_2) \exp(-\pi \tilde{\nu}_1/2)}{4} \left(\frac{2}{3\mu-1} \right)^{\nu_2} \sqrt{3\mu-1} \left| \frac{(\pi + i \cosh(\pi \tilde{\nu}_1) \Gamma(1 - i \tilde{\nu}_1) \Gamma(i \tilde{\nu}_1))}{\pi \Gamma(i \tilde{\nu}_1)} \right| \right)^2$

b. For $\xi = \xi_{\text{cri}}$:

At this junction point, the total energy density at the reheating end is computed as

$$\begin{aligned} \rho_\chi &= \frac{\mathcal{A}_3 H_{\text{end}}^4}{2\pi^2} \ln \left(\frac{k_{\text{end}}}{k_{\text{re}}} \right) \exp(-4N_{\text{re}}) \\ \Rightarrow \rho_\chi &= \frac{\mathcal{A}_3 H_{\text{end}}^4 (1 + 3w_\phi) N_{\text{re}}}{4\pi^2} \exp(-4N_{\text{re}}) \end{aligned} \quad (\text{B4})$$

c. For $\xi > \xi_{\text{cri}}$:

After crossing the critical coupling or the junction ξ_{cri} , the energy spectrum turns out to be red-tilted. The total energy density at the reheating end is now computed as

$$\begin{aligned} \rho_\chi &= \frac{\mathcal{A}_3 H_{\text{end}}^4}{4\pi^2 (\nu_2 - 2)} \left(\frac{k_{\text{end}}}{k_{\text{re}}} \right)^{2\nu_2 - 4} \exp(-4N_{\text{re}}) \\ \Rightarrow \rho_\chi &= \frac{\mathcal{A}_3 H_{\text{end}}^4}{4\pi^2 (\nu_2 - 2)} \exp\left(((1 + 3w_\phi)(\nu_2 - 2) - 4) N_{\text{re}} \right) \end{aligned} \quad (\text{B5})$$

For $0 \leq w_\phi < 1/3$:

4. For $0 \leq \xi < 3/16$

According to the energy density spectrum described in Section II, for $0 \leq w_\phi < 1/3$, we find the existence of a critical coupling ξ_{cri} lying in the range $0 < \xi_{\text{cri}} < 1/6$, below which the energy spectrum is red-tilted and above which the spectrum is blue-tilted. In the entire range $\xi > \xi_{\text{cri}}$, the energy spectrum ρ_{χ_k} remains blue-tilted.

a. For $0 \leq \xi < \xi_{\text{cri}}$:

In the given range, energy spectrum is red-tilted. The total energy density at the reheating end is calculated to be

$$\begin{aligned} \rho_\chi \left(\frac{a}{a_{\text{end}}} \right)^4 &= \frac{\mathcal{A}_1 H_{\text{end}}^4}{2\pi^2} \int_{k_{\text{re}}/k_{\text{end}}}^1 d(k/k_{\text{end}}) (k/k_{\text{end}})^{3-2(\nu_1+\nu_2)} \\ \Rightarrow \rho_\chi &\approx \frac{\mathcal{A}_1 H_{\text{end}}^4}{4\pi^2 ((\nu_1 + \nu_2) - 2)} \exp\left(N_{\text{re}} ((1 + 3w_\phi)(\nu_1 + \nu_2 - 2) - 4) \right) \end{aligned} \quad (\text{B6})$$

b. For $\xi_{\text{cri}} < \xi < 3/16$:

In the given range, energy spectrum is blue-tilted. The total energy density at the reheating end is calculated to be

$$\begin{aligned} \rho_\chi \left(\frac{a}{a_{\text{end}}} \right)^4 &= \frac{\mathcal{A}_1 H_{\text{end}}^4}{2\pi^2} \int_{k_{\text{re}}/k_{\text{end}}}^1 d(k/k_{\text{end}}) (k/k_{\text{end}})^{3-2(\nu_1+\nu_2)} \\ \Rightarrow \rho_\chi &\approx \frac{\mathcal{A}_1 H_{\text{end}}^4}{4\pi^2 (2 - (\nu_1 + \nu_2))} \exp(-4N_{\text{re}}) \end{aligned} \quad (\text{B7})$$

-
- [1] A. H. Guth, *Phys. Rev. D* **23**, 347 (1981).
[2] L. Senatore, in *Theoretical Advanced Study Institute in Elementary Particle Physics: New Frontiers in Fields and Strings* (2017) pp. 447–543, arXiv:1609.00716 [hep-th] .
[3] A. D. Linde, *Phys. Lett. B* **108**, 389 (1982).
[4] A. Albrecht and P. J. Steinhardt, *Phys. Rev. Lett.* **48**, 1220 (1982).
[5] M. Lemoine, J. Martin, and P. Peter, eds., *Inflationary cosmology* (2008).
[6] V. Mukhanov, H. Feldman, and R. Brandenberger, *Physics Reports* **215**, 203 (1992).
[7] J. Martin, *Braz. J. Phys.* **34**, 1307 (2004), arXiv:astro-ph/0312492 .
[8] J. Martin, *Lect. Notes Phys.* **669**, 199 (2005), arXiv:hep-th/0406011 .
[9] A. Linde, in *100e Ecole d'Ete de Physique: Post-Planck Cosmology* (2015) pp. 231–316, arXiv:1402.0526 [hep-th] .
[10] B. A. Bassett, S. Tsujikawa, and D. Wands, *Rev. Mod. Phys.* **78**, 537 (2006).
[11] L. Sriramkumar, (2009), arXiv:0904.4584 [astro-ph.CO] .
[12] D. Baumann and H. V. Peiris, *Adv. Sci. Lett.* **2**, 105 (2009), arXiv:0810.3022 [astro-ph] .
[13] D. Baumann, *PoS TASI2017*, 009 (2018), arXiv:1807.03098 [hep-th] .
[14] O. F. Piattella, *Lecture Notes in Cosmology*, UNITEXT for Physics (Springer, Cham, 2018) arXiv:1803.00070 [astro-ph.CO] .
[15] B. P. Abbott *et al.* (LIGO Scientific, Virgo), *Phys. Rev. Lett.* **116**, 061102 (2016), arXiv:1602.03837 [gr-qc] .
[16] B. P. Abbott *et al.* (LIGO Scientific, Virgo), *Phys. Rev. Lett.* **116**, 131103 (2016), arXiv:1602.03838 [gr-qc] .
[17] B. P. Abbott *et al.* (LIGO Scientific, VIRGO), *Phys. Rev. Lett.* **118**, 221101 (2017), [Erratum: *Phys.Rev.Lett.* 121, 129901 (2018)], arXiv:1706.01812 [gr-qc] .
[18] B. P. Abbott *et al.* (LIGO Scientific, Virgo), *Phys. Rev. Lett.* **118**, 121101 (2017), [Erratum: *Phys.Rev.Lett.* 119, 029901 (2017)], arXiv:1612.02029 [gr-qc] .
[19] Z. Arzoumanian *et al.* (NANOGrav), *Astrophys. J. Lett.* **905**, L34 (2020), arXiv:2009.04496 [astro-ph.HE] .
[20] G. Agazie *et al.* (NANOGrav), *Astrophys. J. Lett.* **951**, L8 (2023), arXiv:2306.16213 [astro-ph.HE] .
[21] G. Agazie *et al.* (NANOGrav), *Astrophys. J. Lett.* **951**, L9 (2023), arXiv:2306.16217 [astro-ph.HE] .
[22] J. Antoniadis *et al.*, (2023), 10.1051/0004-6361/202346841, arXiv:2306.16224 [astro-ph.HE] .
[23] J. Antoniadis *et al.* (EPTA), (2023), arXiv:2306.16214 [astro-ph.HE] .
[24] J. Antoniadis *et al.* (EPTA), (2023), arXiv:2306.16227 [astro-ph.CO] .
[25] D. J. Reardon *et al.*, *Astrophys. J. Lett.* **951**, L6 (2023), arXiv:2306.16215 [astro-ph.HE] .
[26] A. Zic *et al.*, (2023), arXiv:2306.16230 [astro-ph.HE] .
[27] H. Xu *et al.*, *Res. Astron. Astrophys.* **23**, 075024 (2023), arXiv:2306.16216 [astro-ph.HE] .
[28] M. Punturo *et al.*, *Class. Quant. Grav.* **27**, 194002 (2010).
[29] B. Sathyaprakash *et al.*, *Class. Quant. Grav.* **29**, 124013 (2012), [Erratum: *Class.Quant.Grav.* 30, 079501 (2013)], arXiv:1206.0331 [gr-qc] .
[30] J. Crowder and N. J. Cornish, *Phys. Rev. D* **72**, 083005 (2005), arXiv:gr-qc/0506015 .
[31] V. Corbin and N. J. Cornish, *Class. Quant. Grav.* **23**, 2435 (2006), arXiv:gr-qc/0512039 .
[32] J. Baker *et al.*, *Bull. Am. Astron. Soc.* **51**, 243 (2019), arXiv:1907.11305 [astro-ph.IM] .
[33] N. Seto, S. Kawamura, and T. Nakamura, *Phys. Rev. Lett.* **87**, 221103 (2001), arXiv:astro-ph/0108011 .
[34] S. Kawamura *et al.*, *Class. Quant. Grav.* **28**, 094011 (2011).
[35] A. Suemasa, K. Nakagawa, and M. Musha, *Proc. SPIE Int. Soc. Opt. Eng.* **10563**, 105632V (2017).
[36] P. Amaro-Seoane *et al.*, *GW Notes* **6**, 4 (2013), arXiv:1201.3621 [astro-ph.CO] .
[37] E. Barausse *et al.*, *Gen. Rel. Grav.* **52**, 81 (2020), arXiv:2001.09793 [gr-qc] .
[38] G. Janssen *et al.*, *PoS AASKA14*, 037 (2015), arXiv:1501.00127 [astro-ph.IM] .
[39] N. Arkani-Hamed and J. Maldacena, (2015), arXiv:1503.08043 [hep-th] .
[40] X. Chen and Y. Wang, *Phys. Rev. D* **81**, 063511 (2010), arXiv:0909.0496 [astro-ph.CO] .
[41] Y. Akrami *et al.* (Planck), *Astron. Astrophys.* **641**, A10 (2020), arXiv:1807.06211 [astro-ph.CO] .
[42] A. G. Adame *et al.* (DESI), (2024), arXiv:2404.03002 [astro-ph.CO] .
[43] R. Ahumada *et al.* (eBOSS), *Astrophys. J. Suppl.* **249**, 3 (2020), arXiv:1912.02905 [astro-ph.GA] .
[44] V. Faraoni, *Physical Review D* **53**, 6813–6821 (1996).

- [45] S. Tsujikawa, *Phys. Rev. D* **62**, 043512 (2000).
- [46] E. Komatsu and T. Futamase, *Physical Review D* **59** (1999), 10.1103/physrevd.59.064029.
- [47] F. Lucchin, S. Matarrese, and M. Pollock, *Physics Letters B* **167**, 163 (1986).
- [48] B. Spokoiny, *Physics Letters B* **147**, 39 (1984).
- [49] T. Futamase and K.-i. Maeda, *Phys. Rev. D* **39**, 399 (1989).
- [50] M. Shokri, J. Sadeghi, M. R. Setare, and S. Capozziello, *International Journal of Modern Physics D* **30**, 2150070 (2021).
- [51] S. Capozziello and R. de Ritis, *Classical and Quantum Gravity* **11**, 107 (1994).
- [52] K. NOZARI and S. D. SADATIAN, *Modern Physics Letters A* **23**, 2933–2945 (2008).
- [53] C. Gomes, J. Rosa, and O. Bertolami, *Journal of Cosmology and Astroparticle Physics* **2017**, 021–021 (2017).
- [54] P. Sarkar, Ashmita, and P. K. Das, “Non-minimal inflation with a scalar-curvature mixing term $\frac{1}{2}\xi r\phi^2$,” (2023), [arXiv:2205.05532 \[astro-ph.CO\]](#) .
- [55] B. A. Bassett and S. Liberati, *Phys. Rev. D* **58**, 021302 (1998), [Erratum: *Phys.Rev.D* 60, 049902 (1999)], [arXiv:hep-ph/9709417](#) .
- [56] S. Tsujikawa, K.-i. Maeda, and T. Torii, *Phys. Rev. D* **60**, 063515 (1999), [arXiv:hep-ph/9901306](#) .
- [57] S. Tsujikawa, K.-i. Maeda, and T. Torii, *Phys. Rev. D* **60**, 123505 (1999), [arXiv:hep-ph/9906501](#) .
- [58] Y. Ema, R. Jinno, K. Mukaida, and K. Nakayama, *Journal of Cosmology and Astroparticle Physics* **2017**, 045–045 (2017).
- [59] K. Dimopoulos and T. Markkanen, *Journal of Cosmology and Astroparticle Physics* **2018**, 021–021 (2018).
- [60] D. G. Figueroa, A. Florio, T. Opferkuch, and B. A. Stefanek, *SciPost Phys.* **15**, 077 (2023), [arXiv:2112.08388 \[astro-ph.CO\]](#) .
- [61] T. Opferkuch, P. Schwaller, and B. A. Stefanek, *JCAP* **07**, 016 (2019), [arXiv:1905.06823 \[gr-qc\]](#) .
- [62] D. Bettoni, A. Lopez-Eiguren, and J. Rubio, *JCAP* **01**, 002 (2022), [arXiv:2107.09671 \[hep-ph\]](#) .
- [63] G. Laverda and J. Rubio, *JCAP* **03**, 033 (2024), [Erratum: *JCAP* 06, E01 (2024)], [arXiv:2307.03774 \[astro-ph.CO\]](#) .
- [64] D. G. Figueroa and N. Loayza, (2024), [arXiv:2406.02689 \[astro-ph.CO\]](#) .
- [65] G. Laverda and J. Rubio, *JHEP* **05**, 339 (2024), [arXiv:2402.06000 \[hep-ph\]](#) .
- [66] T. Markkanen and S. Nurmi, *JCAP* **02**, 008 (2017), [arXiv:1512.07288 \[astro-ph.CO\]](#) .
- [67] T. Markkanen, *JHEP* **01**, 116 (2018), [arXiv:1711.07502 \[gr-qc\]](#) .
- [68] M. Fairbairn, K. Kainulainen, T. Markkanen, and S. Nurmi, *JCAP* **04**, 005 (2019), [arXiv:1808.08236 \[astro-ph.CO\]](#) .
- [69] K. Kainulainen, O. Koskivaara, and S. Nurmi, *JHEP* **04**, 043 (2023), [arXiv:2209.10945 \[hep-ph\]](#) .
- [70] O. Lebedev, T. Solomko, and J.-H. Yoon, *JCAP* **02**, 035 (2023), [arXiv:2211.11773 \[hep-ph\]](#) .
- [71] E. W. Kolb and A. J. Long, (2023), [arXiv:2312.09042 \[astro-ph.CO\]](#) .
- [72] Y. Ema, K. Nakayama, and Y. Tang, *JHEP* **09**, 135 (2018), [arXiv:1804.07471 \[hep-ph\]](#) .
- [73] Z. Yu, C. Fu, and Z.-K. Guo, *Physical Review D* **108** (2023), 10.1103/physrevd.108.123509.
- [74] J. A. R. Cembranos, L. J. Garay, A. Parra-López, and J. M. Sánchez Velázquez, *JCAP* **02**, 013 (2024), [arXiv:2310.07515 \[gr-qc\]](#) .
- [75] E. W. Kolb and A. J. Long, *JHEP* **03**, 283 (2021), [arXiv:2009.03828 \[astro-ph.CO\]](#) .
- [76] C. Capanelli, L. Jenks, E. W. Kolb, and E. McDonough, (2024), [arXiv:2405.19390 \[hep-th\]](#) .
- [77] C. Capanelli, L. Jenks, E. W. Kolb, and E. McDonough, *Phys. Rev. Lett.* **133**, 061602 (2024), [arXiv:2403.15536 \[hep-th\]](#) .
- [78] M. R. Setare and E. C. Vagenas, *Astrophys. Space Sci.* **330**, 145 (2010), [arXiv:0906.4237 \[gr-qc\]](#) .
- [79] M. Sami, M. Shahalam, M. Skugoreva, A. Toporensky, M. Shahalam, M. Skugoreva, and A. Toporensky, *Phys. Rev. D* **86**, 103532 (2012), [arXiv:1207.6691 \[hep-th\]](#) .
- [80] R. Kase and S. Tsujikawa, *Phys. Rev. D* **101**, 063511 (2020), [arXiv:1910.02699 \[gr-qc\]](#) .
- [81] G. Ye, M. Martinelli, B. Hu, and A. Silvestri, (2024), [arXiv:2407.15832 \[astro-ph.CO\]](#) .
- [82] S. Maiti, D. Maity, and L. Sriramkumar, (2024), [arXiv:2401.01864 \[gr-qc\]](#) .
- [83] S. Cléry, Y. Mambrini, K. A. Olive, A. Shkerin, and S. Verner, *Phys. Rev. D* **105**, 095042 (2022), [arXiv:2203.02004 \[hep-ph\]](#) .
- [84] B. Barman, S. Cléry, R. T. Co, Y. Mambrini, and K. A. Olive, *JHEP* **12**, 072 (2022), [arXiv:2210.05716 \[hep-ph\]](#) .
- [85] A. Ghoshal, D. Paul, and S. Pal, (2024), [arXiv:2405.06741 \[hep-ph\]](#) .
- [86] S. Maity and M. R. Haque, (2024), [arXiv:2407.18246 \[astro-ph.CO\]](#) .
- [87] L. Kofman, A. D. Linde, and A. A. Starobinsky, *Phys. Rev. D* **56**, 3258 (1997), [arXiv:hep-ph/9704452](#) .
- [88] L. Parker and S. A. Fulling, *Phys. Rev. D* **9**, 341 (1974).
- [89] P. R. Anderson and L. Parker, *Phys. Rev. D* **36**, 2963 (1987).
- [90] M. R. de Garcia Maia, *Phys. Rev. D* **48**, 647 (1993).
- [91] N. Aghanim *et al.* (Planck), *Astron. Astrophys.* **641**, A6 (2020), [Erratum: *Astron.Astrophys.* 652, C4 (2021)], [arXiv:1807.06209 \[astro-ph.CO\]](#) .
- [92] L. Dai, M. Kamionkowski, and J. Wang, *Phys. Rev. Lett.* **113**, 041302 (2014).
- [93] A. Afzal, , *et al.*, *The Astrophysical Journal Letters* **951**, L11 (2023).
- [94] L. A. Boyle and P. J. Steinhardt, *Phys. Rev. D* **77**, 063504 (2008), [arXiv:astro-ph/0512014](#) .
- [95] N. D. Birrell and P. C. W. Davies, “Quantum field theory in curved spacetime,” in *Quantum Fields in Curved Space*, Cambridge Monographs on Mathematical Physics (Cambridge University Press, 1982) p. 36–88.
- [96] C. Fu, P. Wu, and H. Yu, *Phys. Rev. D* **97**, 081303 (2018), [arXiv:1711.10888 \[gr-qc\]](#) .
- [97] A. S. Arapoğlu and A. E. Yükselci, *Phys. Dark Univ.* **40**, 101176 (2023), [arXiv:2210.16699 \[gr-qc\]](#) .
- [98] L. Sorbo, *JCAP* **06**, 003 (2011), [arXiv:1101.1525 \[astro-ph.CO\]](#) .

- [99] C. Caprini and L. Sorbo, *JCAP* **10**, 056 (2014), [arXiv:1407.2809 \[astro-ph.CO\]](#) .
- [100] A. Ito and J. Soda, *Phys. Lett. B* **771**, 415 (2017), [arXiv:1607.07062 \[hep-th\]](#) .
- [101] R. Sharma, K. Subramanian, and T. R. Seshadri, *Phys. Rev. D* **101**, 103526 (2020), [arXiv:1912.12089 \[astro-ph.CO\]](#) .
- [102] S. Okano and T. Fujita, *JCAP* **03**, 026 (2021), [arXiv:2005.13833 \[astro-ph.CO\]](#) .
- [103] J. L. Cook and L. Sorbo, *Phys. Rev. D* **85**, 023534 (2012).
- [104] D. G. Figueroa and F. Torrenti, *JCAP* **10**, 057 (2017), [arXiv:1707.04533 \[astro-ph.CO\]](#) .
- [105] M. C. Guzzetti, N. Bartolo, M. Liguori, and S. Matarrese, *Riv. Nuovo Cim.* **39**, 399 (2016), [arXiv:1605.01615 \[astro-ph.CO\]](#) .
- [106] M. R. Haque, D. Maity, T. Paul, and L. Sriramkumar, *Phys. Rev. D* **104**, 063513 (2021), [arXiv:2105.09242 \[astro-ph.CO\]](#) .
- [107] J. J. Bennett, G. Buldgen, P. F. De Salas, M. Drewes, S. Gariazzo, S. Pastor, and Y. Y. Y. Wong, *JCAP* **04**, 073 (2021), [arXiv:2012.02726 \[hep-ph\]](#) .
- [108] J. Froustey, C. Pitrou, and M. C. Volpe, *JCAP* **12**, 015 (2020), [arXiv:2008.01074 \[hep-ph\]](#) .
- [109] K. Akita and M. Yamaguchi, *JCAP* **08**, 012 (2020), [arXiv:2005.07047 \[hep-ph\]](#) .
- [110] M. R. Haque, D. Maity, and R. Mondal, *JHEP* **09**, 012 (2023), [arXiv:2301.01641 \[hep-ph\]](#) .
- [111] A. Chakraborty, M. R. Haque, D. Maity, and R. Mondal, *Phys. Rev. D* **108**, 023515 (2023), [arXiv:2304.13637 \[astro-ph.CO\]](#) .
- [112] C. Caprini and D. G. Figueroa, *Class. Quant. Grav.* **35**, 163001 (2018), [arXiv:1801.04268 \[astro-ph.CO\]](#) .
- [113] T. J. Clarke, E. J. Copeland, and A. Moss, *JCAP* **10**, 002 (2020), [arXiv:2004.11396 \[astro-ph.CO\]](#) .
- [114] T. L. Smith, E. Pierpaoli, and M. Kamionkowski, *Phys. Rev. Lett.* **97**, 021301 (2006), [arXiv:astro-ph/0603144](#) .